

INFRARED ABSORPTION AND EMISSION SPECTRA OF SiO

J. M. CAMPBELL,¹ D. Klapstein,² M. DULICK, AND P. F. BERNATH³

Centre for Molecular Beams and Laser Chemistry, Department of Chemistry, University of Waterloo, Waterloo, Ontario, N2L 3G1, Canada

AND

L. WALLACE

Kitt Peak National Observatory, National Optical Astronomy Observatories, P.O. Box 26732, Tucson, AZ 85726

Received 1995 March 6; accepted 1995 May 1

ABSTRACT

High-resolution Fourier transform infrared spectra of SiO were recorded from two sources, the umbral region of a sunspot and a high-temperature laboratory cell. Rovibrational transitions in the sunspot absorption spectrum were measured in consecutive vibrational bands from (1, 0) to (13, 12) with J values as high as 141 for $^{28}\text{Si}^{16}\text{O}$ (1258 lines) and (1, 0) to (6, 5) for $^{29}\text{Si}^{16}\text{O}$ and $^{30}\text{Si}^{16}\text{O}$ (455 lines). In the lower temperature laboratory emission spectrum only 387 rotational lines in the (1, 0) to (5, 4) bands were measured exclusively for $^{28}\text{Si}^{16}\text{O}$. The laboratory spectrum served primarily to calibrate the lines in the sunspot spectrum to absolute rest frequencies. An improved set of Dunham constants for the $^1\Sigma^+$ ground state was obtained from a global fit of a combined data set consisting of our IR data and all the previously reported microwave and millimeter-wave data. In addition, an internuclear potential for the $^1\Sigma^+$ ground state, in the form of a parameterized modified-Morse function, was also obtained by fitting the data directly to the eigenvalues of the radial Schrödinger equation.

Subject heading: line identification — molecular data

1. INTRODUCTION

The first laboratory microwave spectrum of SiO was recorded by Törring (1968), while the detection of interstellar SiO microwave emission was first reported by Wilson et al. (1971). The astonishing discovery of interstellar SiO maser emission from the Orion nebula by Snyder & Buhl (1974) prompted a systematic search for SiO maser and thermal emission in a variety of different stellar and interstellar sources. One eventual outcome of this extensive search led to cataloguing almost 200 stellar sources (Engels & Heske 1989). Of equal significance was the detection of maser emission arising out of highly excited rovibronic levels. Consequently, the motivation behind the recording of millimeter-wave spectra by Manson et al. (1977), and more recently by Mollaaghbabab et al. (1991) was to determine accurate molecular constants for the $X^1\Sigma^+$ ground state to facilitate the identification of additional SiO maser transitions from astronomical sources.

In spite of the wealth of information on SiO maser emission accumulated over the past two decades, the underlying mechanism responsible for maintaining population inversion to sustain SiO maser oscillation is still not well understood. Geballe & Townes (1974) proposed coincidence rovibronic pumping and IR emission-reabsorption as two possible mechanisms while Kwan & Scoville (1974) have argued in favor of radiative trapping as a means of supporting population inversion. Al-

though these proposed mechanisms are able to account for the maser transitions that were discovered originally, they are, however, unable to explain masing out of higher rovibronic levels that have been observed more recently. Obviously the infrared emission spectrum of SiO plays a key role in unraveling the mechanism responsible for population inversion.

Lovas, Maki, & Olson (1981) recorded the first high-resolution laboratory IR spectrum, the 2–0 vibrational overtone, with the use of a tunable diode laser. All other reports of SiO IR spectra in the gas phase were obtained from stellar sources such as circumstellar shells (Cudaback, Gaustad, & Knacke 1971; Beer, Lambert, & Sneden 1974; Geballe, Lacy, & Beck 1979) or the photospheres of late-type stars (Wollman et al. 1973; Hinkle et al. 1976; Rinsland & Wing 1982).

Another astronomical source for SiO IR spectra have been sunspots. Gaur, Pande, & Tripathi (1972, 1978) were the first to predict SiO in sunspot spectra. In subsequent studies by Glenar et al. (1983, 1985) high-resolution spectra of SiO from the umbral regions of sunspots were recorded utilizing two different approaches: the first of which involved a ground-based tunable diode laser absorption heterodyne spectrometer and the second of which involved the Fourier transform spectrometer (FTS) at the McMath Solar Telescope in Kitt Peak. It was their Fourier transform spectrum that enabled Glenar and coworkers to assemble the most comprehensive list of SiO IR lines to date; almost close to 600 lines from the (1–0) to (10–9) bands of ^{28}SiO and ~ 400 lines from the (1–0) to (4–3) bands of ^{29}SiO and ^{30}SiO . Due to atmospheric absorption, virtually all of their measured lines were P -branch transitions.

In this paper we report on the analysis of a new SiO IR sunspot spectrum that was also obtained with the FTS at the McMath Solar Telescope. To circumvent problems associated with converting observed frequencies in the sunspot spectrum

¹ Present address: University of British Columbia, Department of Chemistry, 2036 Main Mall, Vancouver, British Columbia, V6T 1Y6, Canada.

² Permanent address: St. Francis Xavier University, Chemistry Department, Antigonish, Nova Scotia, B2G 2W5 Canada.

³ Also: Department of Chemistry, University of Arizona.

to rest frequencies, we recorded a second Fourier transform spectrum of SiO in the laboratory, which was then utilized in directly calibrating the SiO lines measured in the sunspot spectrum to absolute rest frequencies.

2. EXPERIMENTAL DETAILS

The sunspot spectrum was obtained in 1982 March at an unapodized resolution of 0.0050 cm^{-1} . The spectrum exhibited pronounced absorption of SiO lines by a factor of at least 2 more than previously recorded sunspot spectra in the $900\text{--}1300\text{ cm}^{-1}$ region. The sunspot was large and observational conditions were excellent, so photospheric contamination was minimal. In addition, the spot was cooler than average, having an excitation temperature of 3200 K , as opposed to the 3700 K reported by Glenar et al. (1985). Most of the measured lines fall between 1070 and 1233 cm^{-1} ; at higher frequencies, atmospheric absorption, primarily by CH_4 , blocks out most of the *R*-branch lines. At the lower frequency end, O_3 absorption extends from ~ 1000 to 1070 cm^{-1} but some high-*J* *P*-branch lines can be traced out through the O_3 band to $\sim 930\text{ cm}^{-1}$. A complete description and analysis of the sunspot spectrum, which makes use of the results of the present work, is given by Wallace, Livingston, & Bernath (1994).

The laboratory spectrum of SiO was obtained with a Bruker IFS 120 HR Fourier transform spectrometer at the University of Waterloo. The spectrum was recorded in emission with a KBr beam splitter, a HgCdTe detector, and a cell temperature of 1400°C . The cell used in the experiment consisted of a 1.2 m long mullite tube with water-cooled KBr end windows, situated inside of a commercial CM Rapid Temp furnace. In actuality, SiO was discovered purely by accident as an impurity in the process of obtaining a GaD spectrum by reacting molten gallium metal with deuterium gas (Campbell et al. 1993). Mullite, $3\text{Al}_2\text{O}_3 \cdot 2\text{SiO}_2$, a refractory material, is not expected to undergo appreciable thermal decomposition at 1400°C . The most obvious explanation for the presence of SiO in the gas-phase seems to be a chemical reaction between molten gallium and mullite.

Rotational line positions from both the laboratory and sunspot spectra were measured using the computer program PC-DECOMP, written by J. Brault, which determines the center of a line by fitting the line profile to a Voigt line shape function. In the laboratory spectrum, a total of 387 *P* and *R* lines were assigned in the fundamental $(1, 0)$ band and the $(2, 1)$ to $(5, 4)$ hot bands. Due to the low isotopic abundances of ^{29}Si (4.7%) and ^{30}Si (3.1%) only rotational lines of the most abundant isotopomer $^{28}\text{Si}^{16}\text{O}$ were observed. The presence of impurity H_2O absorption lines in the spectrum provided the means of calibrating the measured line positions in terms of absolute wavenumbers. The precision for the strongest and sharpest rotational lines measured in the laboratory spectrum is estimated to be 0.0004 cm^{-1} , which was based on both the internal consistency of the calibrated line positions and the spectral linewidth-to signal-to-noise (S/N) ratios. A list of all our measured laboratory $^{28}\text{Si}^{16}\text{O}$ lines is given in Table 1.

In contrast to the laboratory emission spectrum a significantly greater number of rotational lines were assigned in the sunspot absorption spectrum with the sharpest and most intense lines measured to a precision of 0.0006 cm^{-1} . Specifi-

cally, a total of 1713 rotational lines, comprised mainly of *P*-branch lines, were measured involving $\Delta v = +1$ transitions; *R*-branch lines associated with the lower vibrational levels were not observed for the most part due to the transmission cutoff by Earth's atmosphere, which occurs around 1240 cm^{-1} . In terms of individual isotopomers, 1258 lines were assigned in the $(1, 0)$ to $(13, 12)$ bands of $^{28}\text{Si}^{16}\text{O}$ while 277 and 178 *P* and *R* line assignments were obtained from the respective $(1, 0)$ to $(6, 5)$ bands of the minor isotopomers $^{29}\text{Si}^{16}\text{O}$ and $^{30}\text{Si}^{16}\text{O}$. The sunspot data were calibrated by selecting only the strongest lines common to both the laboratory and sunspot spectra and fitting the wavenumbers of these selected set of lines to

$$\nu_{\text{lab}} = b\nu_{\text{sunspot}} \quad (1)$$

to determine the calibration constant *b*. A least-squares fit of 105 selected lines yielded $b = 1.0000057383(264)$. The list of the calibrated SiO sunspot data is given in Table 2.

3. ANALYSIS

The analysis consisted of performing two separate global fits of the SiO data, the listed lines in Tables 1 and 2 and the pure rotational transitions measured by Törring (1968), Manson et al. (1977), and Mollaaghababa et al. (1991) (see Table 3). Below is a description of the analysis that involved two models in reducing the data to molecular constants.

3.1. Mass-reduced Dunham Constants

The first phase of the analysis involved fitting the data to the Dunham energy levels (Dunham 1932)

$$E(v, J) = \sum_{i,j} \mu^{-(i+2j)/2} U_{ij} [1 + (m_e/M_A) \Delta_{ij}^A + (m_e/M_B) \Delta_{ij}^B] (v + \frac{1}{2})^i [J(J+1)]^j, \quad (2)$$

where U_{ij} are mass-reduced Dunham constants, Δ_{ij} are empirical Ross-Watson parameters that correct for breakdown in the Born-Oppenheimer approximation on the silicon (A) and oxygen (B) centers (Ross, Eng, & Kildal 1974; Watson 1973, 1980), μ is the reduced mass, M_A and M_B are the silicon and oxygen atomic masses, and m_e is the electron mass.

Derived parameter values from the fit are given in Table 4 and the residuals for the individual transitions are given in Tables 1–3. Uncertainties in the adjusted parameters are quoted to 1σ . The standard deviation of the weighted least-squares fit,

$$\sqrt{\frac{1}{N-M} \sum_{i=1}^N \left(\frac{\nu_i(\text{observed}) - \nu_i(\text{calculated})}{w_i} \right)^2}, \quad (3)$$

was 0.8579. In equation (3) w_i is the weighting factor, $N (=2186)$ is the number of transitions, and $M (=9)$ is the number of adjustable parameters.

The adopted weighting scheme was as follows: in the laboratory spectrum 68% of the lines were assigned a weighting factor of 0.0004 cm^{-1} , whereas in the sunspot spectrum, the weighting factor for 67% of the ^{28}SiO lines was 0.0006 cm^{-1} and 0.0008 cm^{-1} for 73% and 80% of the much weaker ^{29}SiO and ^{30}SiO lines, respectively. For the pure rotational transitions,

TABLE 1
LABORATORY $^{28}\text{Si}^{16}\text{O}$ LINES^a

Line	Observed	δ	Line	Observed	δ	Line	Observed	δ	Line	Observed	δ	Line	Observed	δ
(1, 0) Band														
P(70)	1105.2669	-3	P(69)	1107.3540	8	P(68)	1109.4314	7	P(67)	1111.4998	0	P(66)	1113.5608	4
P(64)	1117.6561	2	P(63)	1119.6908	0	P(62)	1121.7171	-1	P(61)	1123.7355	5	P(60)	1125.7438	-3
P(59)	1127.7443	-2	P(58)	1129.7358	-5	P(57)	1131.7193	-1	P(56)	1133.6939	2	P(55)	1135.6595	1
P(54)	1137.6180	18	P(53)	1139.5644	1	P(52)	1141.5034	-1	P(51)	1143.4338	-1	P(50)	1145.3551	-3
P(49)	1147.2682	1	P(48)	1149.1717	-1	P(47)	1151.0670	3	P(46)	1152.9525	0	P(45)	1154.8293	0
P(44)	1156.6971	-2	P(43)	1158.5561	0	P(42)	1160.4061	2	P(41)	1162.2467	1	P(40)	1164.0781	-1
P(39)	1165.9009	1	P(38)	1167.7141	0	P(37)	1169.5183	-1	P(36)	1171.3134	1	P(35)	1173.0992	0
P(34)	1174.8757	0	P(33)	1176.6433	3	P(32)	1178.4010	0	P(31)	1180.1496	-2	P(30)	1181.8894	3
P(29)	1183.6193	1	P(28)	1185.3401	3	P(27)	1187.0513	3	P(26)	1188.7530	1	P(25)	1190.4454	1
P(24)	1192.1281	0	P(23)	1193.8013	-3	P(22)	1195.4655	0	P(21)	1197.1200	2	P(20)	1198.7644	-2
P(19)	1200.3997	-1	P(18)	1202.0253	0	P(17)	1203.6416	3	P(16)	1205.2479	3	P(15)	1206.8441	-1
P(14)	1208.4313	2	P(13)	1210.0087	4	P(12)	1211.5757	1	P(11)	1213.1334	2	P(10)	1214.6814	4
P(9)	1216.2191	1	P(8)	1217.7469	-3	P(7)	1219.2656	2	P(6)	1220.7740	2	P(5)	1222.2720	-2
P(4)	1223.7578	-29	R(1)	1232.4808	-6	R(2)	1233.8992	-5	R(3)	1235.3074	-3	R(4)	1236.7061	5
R(5)	1238.0933	0	R(6)	1239.4710	3	R(7)	1240.8378	-2	R(8)	1242.1953	3	R(9)	1243.5420	3
R(10)	1244.8778	-4	R(11)	1246.2044	2	R(12)	1247.5203	3	R(13)	1248.8256	2	R(14)	1250.1205	2
R(15)	1251.4048	0	R(17)	1253.9426	1	R(18)	1255.1958	2	R(19)	1256.4385	3	R(20)	1257.6704	1
R(21)	1258.8917	0	R(22)	1260.1026	0	R(23)	1261.3030	1	R(29)	1268.2801	1	R(30)	1269.4051	-1
R(31)	1270.5199	3	R(32)	1271.6234	2	R(33)	1272.7158	-1	R(34)	1273.7976	-1	R(35)	1274.8686	-1
R(36)	1275.9289	2	R(37)	1276.9778	0	R(38)	1278.0159	1	R(40)	1280.0593	5	R(41)	1281.0637	-1
R(42)	1282.0580	3	R(43)	1283.0407	3	R(44)	1284.0123	3	R(45)	1284.9722	-3	R(46)	1285.9219	0
R(47)	1286.8597	-2	R(48)	1287.7869	0	R(49)	1288.7023	-2	R(50)	1289.6069	1	R(51)	1290.5000	2
R(52)	1291.3818	2	R(53)	1292.2516	-4	R(54)	1293.1113	3	R(55)	1293.9586	0	R(56)	1294.7946	-2
R(57)	1295.6191	-3	R(58)	1296.4334	7	R(59)	1297.2346	1	R(60)	1298.0242	-5	R(61)	1298.8038	5
R(62)	1299.5727	22	R(63)	1300.3251	-8	R(64)	1301.0691	-7	R(65)	1301.8018	-3	R(66)	1302.5223	-3
R(67)	1303.2318	3	R(69)	1304.6129	-11	R(70)	1305.2880	3	R(71)	1305.9486	-9	R(72)	1306.5993	-2
R(73)	1307.2374	-2	R(74)	1307.8656	17	R(75)	1308.4797	14	R(76)	1309.0805	-2	R(77)	1309.6717	4
R(78)	1310.2490	-8	R(81)	1311.9139	5									
(2, 1) Band														
P(67)	1100.3013	2	P(65)	1104.3925	1	P(64)	1106.4258	6	P(63)	1108.4493	-2	P(62)	1110.4648	-3
P(61)	1112.4725	2	P(60)	1114.4714	7	P(59)	1116.4608	2	P(58)	1118.4419	1	P(57)	1120.4146	3
P(56)	1122.3769	-11	P(55)	1124.3332	2	P(54)	1126.2790	-3	P(53)	1128.2167	-1	P(52)	1130.1459	5
P(51)	1132.0656	3	P(50)	1133.9762	-1	P(49)	1135.8783	-1	P(48)	1137.7719	3	P(47)	1139.6523	-36
P(46)	1141.5313	1	P(45)	1143.3977	1	P(44)	1145.2555	5	P(43)	1147.1034	1	P(41)	1150.7726	-3
P(40)	1152.5940	-1	P(39)	1154.4063	1	P(38)	1156.2089	-2	P(37)	1158.0027	-2	P(36)	1159.7873	-2
P(35)	1161.5632	4	P(34)	1163.3292	1	P(33)	1165.0860	1	P(32)	1166.8336	0	P(31)	1168.5728	9
P(30)	1170.3006	-3	P(29)	1172.0208	1	P(28)	1173.7310	0	P(27)	1175.4320	1	P(26)	1177.1236	2
P(25)	1178.8054	0	P(24)	1180.4781	0	P(23)	1182.1414	2	P(22)	1183.7951	3	P(21)	1185.4390	2
P(20)	1187.0736	2	P(19)	1188.6986	2	P(18)	1190.3140	3	P(17)	1191.9200	7	P(16)	1193.5154	-1
P(15)	1195.1024	6	P(14)	1196.6757	-28	P(13)	1198.2454	0	P(12)	1199.8025	-1	P(11)	1201.3502	1
P(10)	1202.8871	-6	P(9)	1204.4155	-1	P(8)	1205.9337	2	R(6)	1227.5061	-1	R(7)	1228.8634	-1
R(8)	1230.2108	3	R(9)	1231.5472	0	R(10)	1232.8759	22	R(11)	1234.1902	3	R(12)	1235.4956	0
R(13)	1236.7912	1	R(14)	1238.0761	0	R(15)	1239.3507	0	R(16)	1240.6146	-2	R(17)	1241.8689	3
R(18)	1243.1121	3	R(19)	1244.3446	1	R(20)	1245.5667	0	R(21)	1246.7782	0	R(22)	1247.9793	0
R(23)	1249.1697	0	R(24)	1250.3494	0	R(25)	1251.5187	1	R(27)	1253.8249	1	R(28)	1254.9620	3
R(29)	1256.0880	0	R(30)	1257.2035	0	R(31)	1258.3084	3	R(32)	1259.4018	-1	R(33)	1260.4853	4
R(34)	1261.5572	2	R(39)	1266.7533	-2	R(41)	1268.7553	2	R(42)	1269.7391	-3	R(43)	1270.7128	4
R(44)	1271.6743	-1	R(45)	1272.6255	2	R(46)	1273.5650	0	R(47)	1274.4933	-1	R(48)	1275.4107	1
R(49)	1276.3171	5	R(50)	1277.2115	1	R(51)	1278.0950	1	R(52)	1278.9660	-9	R(53)	1279.8279	1
R(54)	1280.6774	2	R(55)	1281.5148	-4	R(57)	1283.1570	0	R(58)	1283.9606	-1	R(59)	1284.7533	4
R(60)	1285.5329	-7	R(61)	1286.3032	5	R(62)	1287.0604	1	R(63)	1287.8062	0	R(64)	1288.5409	2
R(65)	1289.2640	6	R(66)	1289.9742	-3	R(67)	1290.6732	-6	R(69)	1292.0382	8	R(70)	1292.7010	-5
R(71)	1293.3547	8	R(72)	1293.9937	-8	R(73)	1294.6244	12	R(74)	1295.2396	-4			

TABLE 1—Continued

Line	Observed	δ	Line	Observed	δ	Line	Observed	δ	Line	Observed	δ	Line	Observed	δ
(3, 2) Band														
P(71)	1080.8966	7	P(59)	1105.2120	3	P(58)	1107.1828	5	P(57)	1109.1443	1	P(56)	1111.0972	-2
P(55)	1113.0419	1	P(54)	1114.9772	-4	P(53)	1116.9045	1	P(52)	1118.8225	-1	P(51)	1120.7310	-9
P(50)	1122.6330	6	P(48)	1126.4071	4	P(47)	1128.2803	-2	P(46)	1130.1459	6	P(45)	1132.0014	2
P(44)	1133.8488	7	P(43)	1135.6862	2	P(42)	1137.5154	5	P(41)	1139.3353	6	P(40)	1141.1449	-6
P(39)	1142.9472	1	P(38)	1144.7398	2	P(37)	1146.5234	4	P(36)	1148.2973	1	P(35)	1150.0620	-2
P(34)	1151.8182	2	P(33)	1153.5648	3	P(32)	1155.3019	1	P(31)	1157.0305	7	P(30)	1158.7486	1
P(29)	1160.4609	31	P(28)	1162.1580	2	P(27)	1163.8483	-2	P(26)	1165.5295	-1	P(25)	1167.2037	23
P(24)	1168.8637	0	P(23)	1170.5168	2	P(22)	1172.1595	-4	P(21)	1173.7938	1	P(20)	1175.4184	4
P(19)	1177.0331	4	P(18)	1178.6382	4	P(17)	1180.2333	0	P(14)	1184.9621	2	R(12)	1223.5076	1
R(15)	1227.3296	-32	R(16)	1228.5879	9	R(17)	1229.8312	4	R(18)	1231.0642	0	R(19)	1232.2873	3
R(20)	1233.4989	-4	R(21)	1234.7015	5	R(22)	1235.8926	3	R(23)	1237.0726	-2	R(24)	1238.2426	-2
R(25)	1239.4022	1	R(26)	1240.5510	3	R(27)	1241.6882	-4	R(28)	1242.8159	0	R(29)	1243.9325	2
R(30)	1245.0379	-1	R(31)	1246.1332	3	R(32)	1247.2173	4	R(33)	1248.2901	-1	R(34)	1249.3527	2
R(35)	1250.4042	2	R(36)	1251.4439	-6	R(37)	1252.4742	0	R(38)	1253.4936	8	R(39)	1254.5006	1
R(40)	1255.4974	3	R(41)	1256.4828	2	R(42)	1257.4576	4	R(43)	1258.4212	5	R(44)	1259.3735	5
R(45)	1260.3141	0	R(46)	1261.2452	10	R(48)	1263.0698	-9	R(49)	1263.9672	1	R(53)	1267.4391	-6
R(54)	1268.2801	5	R(55)	1269.1073	-7	R(56)	1269.9247	-3	R(58)	1271.5243	-5	R(59)	1272.3074	0
R(60)	1273.0780	-6	R(61)	1273.8393	11	R(63)	1275.3233	6	R(65)	1276.7609	1	R(67)	1278.1541	18
R(72)	1281.4227	-28												
(4, 3) Band														
P(52)	1107.5330	-18	P(51)	1109.4314	-21	P(50)	1111.3229	-6	P(49)	1113.2049	2	P(44)	1122.4762	-3
P(43)	1124.3046	7	P(41)	1127.9307	-10	P(39)	1131.5236	3	P(38)	1133.3051	-2	P(36)	1136.8427	6
P(35)	1138.5968	0	P(34)	1140.3415	-7	P(33)	1142.0779	-5	P(32)	1143.8054	1	P(31)	1145.5234	4
R(31)	1233.9935	-1	R(32)	1235.0675	-4	R(33)	1236.1312	-2	R(34)	1237.1840	0	R(36)	1239.2570	5
R(37)	1240.2770	6	R(38)	1241.2859	5	R(39)	1242.2831	-2	R(40)	1243.2708	5	R(41)	1244.2468	6
R(42)	1245.2114	4	R(43)	1246.1657	9	R(44)	1247.1071	-3	R(45)	1248.0391	1	R(46)	1248.9591	-3
R(47)	1249.8697	12	R(48)	1250.7670	5									
(5, 4) Band														
P(60)	1080.8556	-46	P(51)	1098.1751	52	P(42)	1114.7650	3	P(37)	1123.6674	-14	P(33)	1130.6262	-12
P(29)	1137.4379	-3	P(28)	1139.1176	1	P(23)	1147.3753	17						

^a Observed – calculated residuals (δ) are in units of 0.0001 cm⁻¹.

weights of 3×10^{-6} cm⁻¹ were assigned to transitions measured by Törring and 7×10^{-6} cm⁻¹ to transitions measured by Manson et al. The transitions measured by Mollaaghbababa et al. ranging from $v = 0$ to $v = 40$ required a progressive weighting scheme to reflect the gradual degradation in the S/N ratio (cf. the spectra displayed in Fig. 2 of Mollaaghbababa et al. [1991]), which is inversely related to the accuracy of determining the center of a line. The weighting function that we chose,

$$w(v) = \exp [-12.896 + 0.0513(v + \frac{1}{2})], \quad (4)$$

is similar in form to a Boltzmann factor with respective lower and upper limits of $w(0) = 3 \times 10^{-6}$ cm⁻¹ and $w(40) = 2 \times 10^{-5}$ cm⁻¹. Values of $w(v)$ in between these two limits were rounded off to one significant digit to simulate a staircase-like weighting scheme.

In fitting the data to equation (2), only the values of U_{ij} where $j = 0, 1$ were treated as adjustable parameters. The re-

maining values of U_{ij} were computed at the start of each iteration cycle of the least-squares calculation by using analytical relationships between the dependent U_{ij} 's ($j \geq 2$) and the independent U_{ij} 's ($j \leq 1$) (Watson 1980; Ogilvie 1983; Tyuterev & Velichko 1984). To appreciate just how superior this type of fit really is, as opposed to the more traditional approach of treating all the values of U_{ij} as adjustable parameters, consider the following trial fit where the traditional approach was tried. Fifteen values of U_{ij} were determined,

$$U_{i0} \quad 1 \leq i \leq 4, \quad U_{i1} \quad 0 \leq i \leq 4, \quad U_{i2} \quad 0 \leq i \leq 3, \quad U_{i3} \quad 0 \leq i \leq 1,$$

and the standard deviation was 0.8603, as compared to 0.8579 for the fit with constraints that required only nine adjustable parameters.

Because the data convey only isotopic information about the silicon center, the Δ_{ij}^O parameters were automatically fixed to zero. Results from the fit also indicated that the data were not sensitive to breakdown in the Born-Oppenheimer approxima-

TABLE 2
SUNSPOT SiO LINES^a

Line	Observed	δ	Line	Observed	δ	Line	Observed	δ	Line	Observed	δ	Line	Observed	δ
²⁸ Si ¹⁶ O														
(1, 0) Band														
P(141)	936.9546	13	P(138)	944.8216	5	P(137)	947.4301	3	P(133)	957.7940	-6	P(132)	960.3668	-15
P(131)	962.9348	1	P(129)	968.0462	-2	P(128)	970.5914	-1	P(127)	973.1300	4	P(125)	978.1841	2
P(124)	980.7007	4	P(123)	983.2110	16	P(122)	985.7103	-10	P(121)	988.2036	-23	P(120)	990.6938	6
P(116)	1000.5682	-6	P(115)	1003.0184	-8	P(114)	1005.4624	2	P(112)	1010.3248	-10	P(111)	1012.7441	-22
P(110)	1015.1598	4	P(108)	1019.9644	15	P(103)	1031.8372	-13	P(102)	1034.1908	2	P(98)	1043.5221	3
P(97)	1045.8363	11	P(88)	1066.3015	6	P(85)	1072.9797	5	P(84)	1075.1895	3	P(83)	1077.3914	3
P(81)	1081.7700	-4	P(80)	1083.9479	1	P(79)	1086.1171	1	P(78)	1088.2786	6	P(77)	1090.4309	1
P(74)	1096.8395	2	P(73)	1098.9588	0	P(72)	1101.0701	1	P(71)	1103.1722	-6	P(70)	1105.2676	4
P(69)	1107.3531	-1	P(68)	1109.4323	16	P(66)	1113.5613	9	P(65)	1115.6130	6	P(64)	1117.6556	-3
P(63)	1119.6915	6	P(62)	1121.7169	-3	P(61)	1123.7350	1	P(60)	1125.7440	-1	P(58)	1129.7348	-16
P(57)	1131.7195	1	P(56)	1133.6938	1	P(54)	1137.6157	-5	P(53)	1139.5642	-1	P(52)	1141.5034	-1
P(51)	1143.4326	-13	P(50)	1145.3559	4	P(49)	1147.2683	2	P(48)	1149.1721	3	P(47)	1151.0667	0
P(46)	1152.9533	8	P(45)	1154.8295	2	P(44)	1156.6975	2	P(43)	1158.5563	2	P(42)	1160.4059	0
P(41)	1162.2471	5	P(40)	1164.0780	-3	P(39)	1165.9009	1	P(38)	1167.7146	4	P(37)	1169.5195	12
P(36)	1171.3135	2	P(35)	1173.0994	2	P(34)	1174.8761	3	P(33)	1176.6437	7	P(32)	1178.4020	10
P(31)	1180.1496	-1	P(30)	1181.8891	0	P(29)	1183.6195	3	P(28)	1185.3400	2	P(25)	1190.4454	1
P(24)	1192.1276	-6	P(23)	1193.8016	1	P(22)	1195.4662	7	P(21)	1197.1194	-4	P(20)	1198.7645	-1
P(19)	1200.4001	4	P(18)	1202.0255	1	P(17)	1203.6416	3	P(16)	1205.2478	3	P(15)	1206.8448	6
P(14)	1208.4313	2	P(13)	1210.0076	-6	P(12)	1211.5757	1	P(11)	1213.1327	-6	P(10)	1214.6810	0
P(8)	1217.7503	32	P(7)	1219.2626	-28	P(6)	1220.7731	-7	P(5)	1222.2723	1	P(4)	1223.7604	-3
P(2)	1226.7064	-14	P(1)	1228.1656	-7									
(2, 1) Band														
P(141)	926.5650	3	P(140)	929.1778	-53	P(138)	934.3987	-4	P(136)	939.5876	4	P(135)	942.1713	4
P(133)	947.3225	55	P(132)	949.8787	-9	P(131)	952.4351	2	P(130)	954.9832	-1	P(129)	957.5253	8
P(128)	960.0589	4	P(127)	962.5855	1	P(126)	965.1065	13	P(124)	970.1258	28	P(121)	977.5952	-2
P(120)	980.0696	-20	P(119)	982.5404	0	P(118)	985.0007	-14	P(117)	987.4597	34	P(116)	989.9036	6
P(115)	992.3432	8	P(114)	994.7738	-6	P(112)	999.6159	-1	P(111)	1002.0263	8	P(110)	1004.4276	0
P(109)	1006.8230	9	P(108)	1009.2094	4	P(92)	1046.3558	4	P(89)	1053.0972	0	P(85)	1061.9747	3
P(84)	1064.1737	2	P(83)	1066.3649	3	P(81)	1070.7216	-6	P(80)	1072.8893	4	P(79)	1075.0475	2
P(77)	1079.3395	1	P(76)	1081.4733	1	P(75)	1083.5989	3	P(74)	1085.7160	3	P(73)	1087.8246	1
P(71)	1092.0158	-12	P(70)	1094.1009	3	P(69)	1096.1757	-2	P(66)	1102.3511	2	P(65)	1104.3926	2
P(64)	1106.4255	3	P(63)	1108.4496	2	P(62)	1110.4653	1	P(61)	1112.4719	-3	P(60)	1114.4705	-3
P(59)	1116.4610	4	P(58)	1118.4418	1	P(57)	1120.4140	-2	P(56)	1122.3784	3	P(54)	1126.2795	2
P(53)	1128.2166	-2	P(51)	1132.0652	-1	P(50)	1133.9763	0	P(47)	1139.6559	0	P(46)	1141.5308	-4
P(45)	1143.3974	-2	P(44)	1145.2555	5	P(43)	1147.1026	-8	P(42)	1148.9436	9	P(41)	1150.7732	2
P(39)	1154.4063	2	P(38)	1156.2087	-4	P(36)	1159.7878	3	P(35)	1161.5624	-5	P(34)	1163.3292	2
P(33)	1165.0865	6	P(32)	1166.8333	-3	P(30)	1170.3024	14	P(29)	1172.0212	6	P(27)	1175.4333	14
P(26)	1177.1233	0	P(25)	1178.8054	0	P(24)	1180.4782	2	P(23)	1182.1409	-3	P(22)	1183.7949	1
P(21)	1185.4390	1	P(19)	1188.6993	10	P(18)	1190.3133	-4	P(17)	1191.9196	3	P(15)	1195.1018	0
P(14)	1196.6790	5	P(12)	1199.8007	-20	P(11)	1201.3510	9	P(10)	1202.8878	0	P(9)	1204.4147	-8
P(8)	1205.9322	-14	P(7)	1207.4434	17	P(6)	1208.9402	2	P(5)	1210.4299	16	P(3)	1213.3759	8
P(2)	1214.8336	0	P(1)	1216.2834	15	R(0)	1219.1516	29	R(1)	1220.5705	36	R(2)	1221.9747	-4
R(4)	1224.7597	-12	R(6)	1227.5061	0	R(7)	1228.8608	-26	R(8)	1230.2117	12	R(9)	1231.5498	25
R(10)	1232.8767	30	R(11)	1234.1917	19	R(12)	1235.4952	-4	R(13)	1236.7903	-8			
(3, 2) Band														
P(133)	936.8721	1	P(132)	939.4210	-24	P(131)	941.9681	3	P(129)	947.0347	-6	P(128)	949.5598	15
P(126)	954.5828	0	P(125)	957.0838	-5	P(124)	959.5791	4	P(123)	962.0655	-2	P(122)	964.5454	0
P(121)	967.0221	41	P(120)	969.4834	2	P(118)	974.3928	11	P(117)	976.8350	2	P(116)	979.2700	-6
P(114)	984.1203	3	P(113)	986.5390	54	P(111)	991.3381	-1	P(109)	996.1128	0	P(97)	1024.1204	-1
P(91)	1037.7059	8	P(89)	1042.1696	-4	P(76)	1070.4057	1	P(74)	1074.6271	4	P(73)	1076.7251	2
P(72)	1078.8145	-1	P(71)	1080.8964	5	P(70)	1082.9690	1	P(69)	1085.0337	2	P(68)	1087.0902	5

TABLE 2—Continued

Line	Observed	δ	Line	Observed	δ	Line	Observed	δ	Line	Observed	δ	Line	Observed	δ
$^{28}\text{Si}^{16}\text{O}$														
(3, 2) Band														
P(67)	1089.1373	0	P(66)	1091.1760	-5	P(65)	1093.2076	3	P(64)	1095.2289	-5	P(63)	1097.2435	4
P(61)	1101.2450	4	P(60)	1103.2329	4	P(59)	1105.2101	-17	P(57)	1109.1444	2	P(56)	1111.0973	-1
P(55)	1113.0425	6	P(53)	1116.9034	-11	P(51)	1120.7318	-1	P(50)	1122.6327	3	P(49)	1124.5237	-3
P(48)	1126.4068	1	P(47)	1128.2805	0	P(45)	1132.0013	1	P(44)	1133.8476	-6	P(42)	1137.5159	10
P(41)	1139.3343	-4	P(40)	1141.1455	0	P(39)	1142.9472	1	P(38)	1144.7396	0	P(37)	1146.5232	2
P(36)	1148.2974	2	P(35)	1150.0628	6	P(34)	1151.8177	-3	P(33)	1153.5652	6	P(32)	1155.3019	1
P(31)	1157.0292	-6	P(30)	1158.7495	10	P(29)	1160.4578	0	P(28)	1162.1580	2	P(27)	1163.8488	3
P(26)	1165.5299	3	P(25)	1167.2020	6	P(24)	1168.8638	1	P(23)	1170.5162	-3	P(22)	1172.1599	0
P(21)	1173.7945	7	P(20)	1175.4172	-8	P(19)	1177.0329	2	P(18)	1178.6373	-5	P(17)	1180.2326	-7
P(16)	1181.8197	6	P(15)	1183.3952	-1	P(14)	1184.9627	8	P(13)	1186.5188	2	P(12)	1188.0657	1
P(11)	1189.6031	1	P(10)	1191.1305	0	P(9)	1192.6479	-3	P(8)	1194.1559	-1	P(6)	1197.1426	5
P(5)	1198.6202	-1	P(4)	1200.0886	0	P(3)	1201.5457	-13	P(2)	1202.9958	5	R(0)	1207.2819	16
R(1)	1208.6858	-28	R(3)	1211.4733	-14	R(4)	1212.8527	1	R(5)	1214.2198	-4	R(6)	1215.5779	2
R(7)	1216.9253	3	R(8)	1218.2612	-9	R(9)	1219.5892	3	R(10)	1220.9058	4	R(11)	1222.2118	2
R(12)	1223.5089	15	R(13)	1224.7938	8	R(15)	1227.3349	22	R(16)	1228.5874	4	R(17)	1229.8281	-27
R(18)	1231.0610	-32	R(19)	1232.2873	3	R(21)	1234.7022	11	R(24)	1238.2461	33	R(25)	1239.4040	20
(4, 3) Band														
P(128)	939.0904	-1	P(127)	941.5952	-2	P(126)	944.0942	11	P(125)	946.5839	2	P(123)	951.5418	-12
P(122)	954.0141	23	P(120)	958.9252	-24	P(118)	963.8140	-1	P(115)	971.0883	-4	P(113)	975.9004	-9
P(112)	978.2976	12	P(111)	980.6840	-2	P(110)	983.0631	-12	P(109)	985.4369	0	P(108)	987.8025	5
P(107)	990.1596	1	P(106)	992.5097	3	P(105)	994.8512	-6	P(103)	999.5138	3	P(102)	1001.8335	6
P(69)	1073.9253	-3	P(67)	1078.0090	8	P(65)	1082.0552	-16	P(64)	1084.0686	2	P(62)	1088.0659	0
P(61)	1090.0521	3	P(59)	1093.9977	0	P(58)	1095.9577	0	P(57)	1097.9094	3	P(56)	1099.8532	15
P(54)	1103.7116	9	P(52)	1107.5349	2	P(51)	1109.4323	-13	P(50)	1111.3225	-10	P(49)	1113.2043	-3
P(48)	1115.0771	3	P(47)	1116.9411	9	P(45)	1120.6401	2	P(42)	1126.1214	-9	P(41)	1127.9318	1
P(40)	1129.7348	27	P(39)	1131.5235	3	P(38)	1133.3074	20	P(37)	1135.0776	-8	P(36)	1136.8429	7
P(35)	1138.5968	-1	P(34)	1140.3420	-3	P(33)	1142.0787	3	P(32)	1143.8054	0	P(31)	1145.5236	5
P(30)	1147.2316	2	P(29)	1148.9289	-15	P(28)	1150.6215	14	P(27)	1152.3000	-4	P(26)	1153.9705	-8
P(25)	1155.6329	1	P(24)	1157.2841	-7	P(23)	1158.9275	0	P(22)	1160.5605	0	P(21)	1162.1844	3
P(20)	1163.7972	-10	P(18)	1166.9976	1	P(16)	1170.1587	2	P(15)	1171.7242	-3	P(14)	1173.2796	-12
P(13)	1174.8275	1	P(12)	1176.3642	-1	P(10)	1179.4093	5	P(8)	1182.4138	-3	P(7)	1183.9028	8
P(6)	1185.3796	-4	P(4)	1188.3066	3	P(3)	1189.7541	-5	P(2)	1191.1922	-7	P(1)	1192.6222	10
R(1)	1196.8461	2	R(3)	1199.6107	-14	R(4)	1200.9795	-4	R(5)	1202.3376	0	R(6)	1203.6858	7
R(7)	1205.0228	3	R(8)	1206.3499	4	R(9)	1207.6664	0	R(10)	1208.9734	5	R(11)	1210.2665	-27
R(12)	1211.5549	-2	R(13)	1212.8299	-8	R(14)	1214.0958	-1	R(15)	1215.3528	21	R(16)	1216.5947	-4
R(17)	1217.8300	10	R(18)	1219.0539	14	R(19)	1220.2643	-12	R(20)	1221.4680	1	R(22)	1223.8422	11
R(24)	1226.1714	-6	R(25)	1227.3198	-17	R(26)	1228.4608	5	R(27)	1229.5912	28	R(28)	1230.7001	-57
R(29)	1231.8172	47	R(30)	1232.9078	-7	R(31)	1233.9924	-12	R(32)	1235.0656	-23	R(33)	1236.1284	-30
R(37)	1240.2763	-1	R(38)	1241.2871	17	R(39)	1242.2868	35						
(5, 4) Band														
P(121)	945.9612	0	P(120)	948.4044	-1	P(119)	950.8396	-9	P(118)	953.2700	7	P(117)	955.6905	0
P(116)	958.1000	-45	P(115)	960.5114	4	P(113)	965.3027	8	P(111)	970.0626	-3	P(110)	972.4324	2
P(109)	974.7949	10	P(108)	977.1473	-9	P(107)	979.4954	6	P(106)	981.8334	-5	P(105)	984.1662	9
P(104)	986.4895	4	P(103)	988.8076	22	P(102)	991.1119	-20	P(101)	993.4149	2	P(98)	1000.2712	2
P(97)	1002.5403	-5	P(94)	1009.3041	6	P(93)	1011.5422	1	P(92)	1013.7718	-10	P(91)	1015.9941	-15
P(89)	1020.4173	0	P(88)	1022.6180	18	P(82)	1035.6406	-6	P(80)	1039.9177	-4	P(79)	1042.0459	16
P(78)	1044.1616	-6	P(77)	1046.2716	-5	P(72)	1056.6974	4	P(71)	1058.7588	17	P(66)	1068.9311	-2
P(65)	1070.9411	3	P(64)	1072.9402	-16	P(62)	1076.9181	0	P(61)	1078.8933	-1	P(60)	1080.8589	-13
P(59)	1082.8187	5	P(58)	1084.7682	5	P(57)	1086.7087	2	P(56)	1088.6401	-4	P(55)	1090.5641	2
P(54)	1092.4804	18	P(53)	1094.3841	-3	P(52)	1096.2819	3	P(51)	1098.1696	-3	P(50)	1100.0495	1
P(49)	1101.9200	-1	P(48)	1103.7821	3	P(46)	1107.4775	-10	P(45)	1109.3151	16	P(44)	1111.1397	2
P(43)	1112.9564	-2	P(42)	1114.7650	3	P(41)	1116.5635	-1	P(40)	1118.3527	-8	P(39)	1120.1344	0

TABLE 2—Continued

Line	Observed	δ	Line	Observed	δ	Line	Observed	δ	Line	Observed	δ	Line	Observed	δ
$^{28}\text{Si}^{16}\text{O}$														
(5, 4) Band														
P(38)	1121.9055	-6	P(37)	1123.6689	2	P(36)	1125.4225	3	P(35)	1127.1665	0	P(34)	1128.9011	-5
P(33)	1130.6284	9	P(32)	1132.3438	-2	P(31)	1134.0514	0	P(28)	1139.1173	-3	P(27)	1140.7880	4
P(26)	1142.4475	-8	P(25)	1144.0994	-1	P(24)	1145.7421	9	P(23)	1147.3735	-1	P(22)	1148.9973	9
P(20)	1152.2137	1	P(19)	1153.8075	-4	P(18)	1155.3927	1	P(17)	1156.9682	5	P(16)	1158.5325	-7
P(15)	1160.0896	6	P(14)	1161.6367	16	P(13)	1163.1722	6	P(12)	1164.6993	9	P(11)	1166.2155	2
P(9)	1169.2202	3	P(8)	1170.7073	-4	P(7)	1172.1870	16	P(6)	1173.6527	-6	P(5)	1175.1113	-1
P(3)	1177.9998	21	R(3)	1187.7837	-12	R(4)	1189.1434	5	R(5)	1190.4905	-1	R(6)	1191.8286	5
R(8)	1194.4735	9	R(9)	1195.7795	0	R(10)	1197.0759	-2	R(11)	1198.3629	5	R(12)	1199.6376	-9
R(13)	1200.9041	0	R(14)	1202.1584	-10	R(15)	1203.4040	-3	R(16)	1204.6395	7	R(17)	1205.8636	8
R(18)	1207.0767	2	R(19)	1208.2798	3	R(20)	1209.4729	8	R(21)	1210.6554	12	R(22)	1211.8264	7
R(23)	1212.9866	0	R(24)	1214.1373	4	R(25)	1215.2766	1	R(26)	1216.4066	10	R(27)	1217.5238	-1
R(29)	1219.7309	25	R(30)	1220.8135	-11	R(32)	1222.9543	-2	R(36)	1227.1042	0	R(37)	1228.1148	4
R(40)	1231.0814	22	R(42)	1233.0023	18	R(43)	1233.9462	16	R(44)	1234.8798	22			
(6, 5) Band														
P(122)	933.0427	11	P(120)	937.9115	-22	P(119)	940.3394	5	P(118)	942.7569	2	P(117)	945.1666	-5
P(114)	952.3543	1	P(112)	957.1087	3	P(110)	961.8331	3	P(109)	964.1837	1	P(108)	966.5262	-8
P(107)	968.8634	6	P(106)	971.1901	-10	P(104)	975.8248	1	P(102)	980.4261	-18	P(101)	982.7184	5
P(100)	985.0007	4	P(99)	987.2748	-1	P(98)	989.5458	41	P(97)	991.8011	3	P(96)	994.0518	-3
P(95)	996.2959	4	P(94)	998.5308	-3	P(90)	1007.3950	0	P(88)	1011.7810	16	P(86)	1016.1345	27
P(85)	1018.2960	1	P(84)	1020.4524	3	P(83)	1022.5991	-10	P(71)	1047.7396	8	P(70)	1049.7815	17
P(69)	1051.8128	3	P(68)	1053.8370	2	P(61)	1067.7690	-3	P(60)	1069.7258	3	P(59)	1071.6732	2
P(58)	1073.6127	8	P(57)	1075.5416	-6	P(55)	1079.3765	-2	P(54)	1081.2808	-1	P(53)	1083.1759	-3
P(52)	1085.0638	9	P(51)	1086.9437	30	P(50)	1088.8092	-5	P(49)	1090.6705	7	P(48)	1092.5175	-37
P(47)	1094.3634	-2	P(46)	1096.1979	8	P(45)	1098.0219	2	P(44)	1099.8379	5	P(43)	1101.6441	1
P(42)	1103.4417	1	P(41)	1105.2309	7	P(40)	1107.0098	0	P(39)	1108.7801	-1	P(38)	1110.5417	1
P(36)	1114.0366	-3	P(35)	1115.7712	2	P(33)	1119.2111	-1	P(31)	1122.6137	-8	P(27)	1129.3095	-2
P(26)	1130.9594	-7	P(24)	1134.2326	1	P(21)	1139.0739	34	P(20)	1140.6642	1	P(19)	1142.2498	16
P(17)	1145.3870	-6	P(16)	1146.9433	4	P(14)	1150.0237	-8	P(12)	1153.0694	20	P(11)	1154.5742	-1
P(9)	1157.5589	1	P(7)	1160.5030	-10	P(6)	1161.9617	-1	P(3)	1166.2765	5	R(0)	1171.8894	5
R(5)	1178.6779	-8	R(9)	1183.9281	2	R(10)	1185.2130	-15	R(11)	1186.4911	2	R(12)	1187.7571	0
R(13)	1189.0135	7	R(14)	1190.2596	14	R(15)	1191.4924	-8	R(16)	1192.7171	-7	R(18)	1195.1353	-4
R(20)	1197.5123	6	R(23)	1200.9964	-3	R(24)	1202.1373	1	R(25)	1203.2687	16	R(26)	1204.3856	-6
R(27)	1205.4943	-5	R(28)	1206.5921	-5	R(29)	1207.6816	18	R(30)	1208.7561	0	R(32)	1210.8765	0
R(34)	1212.9539	3	R(35)	1213.9763	4	R(36)	1214.9883	10	R(37)	1215.9889	11	R(38)	1216.9784	12
R(39)	1217.9560	2	R(40)	1218.9233	0	R(41)	1219.8806	8	R(42)	1220.8283	30	R(47)	1225.3876	14
R(48)	1226.2664	14	R(49)	1227.1322	-3	R(50)	1227.9896	9	R(51)	1228.8339	3	R(52)	1229.6660	-14
R(53)	1230.4896	-2	R(54)	1231.3040	32									
(7, 6) Band														
P(116)	937.0660	-20	P(112)	946.5631	1	P(110)	951.2654	-2	P(109)	953.6068	10	P(106)	960.5823	15
P(105)	962.8901	-5	P(103)	967.4877	1	P(102)	969.7783	38	P(101)	972.0531	-6	P(100)	974.3273	20
P(97)	981.0942	6	P(96)	983.3338	-3	P(95)	985.5683	14	P(94)	987.7908	-10	P(93)	990.0091	3
P(92)	992.2180	0	P(88)	1000.9754	-3	P(86)	1005.3070	3	P(85)	1007.4600	-1	P(83)	1011.7407	-23
P(81)	1015.9941	6	P(80)	1018.1062	-3	P(67)	1044.8262	6	P(65)	1048.8095	-13	P(60)	1058.6257	10
P(56)	1066.3202	-9	P(55)	1068.2236	1	P(54)	1070.1176	4	P(53)	1072.0020	-1	P(52)	1073.8785	2
P(51)	1075.7456	-1	P(50)	1077.6046	3	P(49)	1079.4552	12	P(46)	1084.9497	-3	P(44)	1088.5675	-19
P(43)	1090.3659	2	P(42)	1092.1528	-1	P(41)	1093.9315	3	P(40)	1095.7006	3	P(39)	1097.4609	5
P(38)	1099.2109	-6	P(37)	1100.9532	-3	P(36)	1102.6863	1	P(35)	1104.4106	8	P(34)	1106.1241	-2
P(32)	1109.5255	-1	P(31)	1111.2121	-2	P(30)	1112.8913	15	P(29)	1114.5581	1	P(28)	1116.2175	7
P(27)	1117.8663	-1	P(26)	1119.5063	-2	P(25)	1121.1371	-2	P(24)	1122.7578	-8	P(23)	1124.3700	-5
P(20)	1129.1491	-2	P(19)	1130.7231	-1	P(18)	1132.2876	1	P(16)	1135.3872	-2	P(15)	1136.9237	8
P(13)	1139.9655	5	P(12)	1141.4723	9	P(11)	1142.9704	22	P(9)	1145.9347	22	P(3)	1154.5895	2

TABLE 2—Continued

Line	Observed	δ	Line	Observed	δ	Line	Observed	δ	Line	Observed	δ	Line	Observed	δ
$^{28}\text{Si}^{16}\text{O}$														
(7, 6) Band														
R(1)	1161.5294	-8	R(2)	1162.8881	-3	R(3)	1164.2352	-11	R(6)	1168.2197	1	R(8)	1170.8248	5
R(9)	1172.1113	0	R(10)	1173.3880	-1	R(12)	1175.9107	0	R(13)	1177.1575	9	R(15)	1179.6172	0
R(16)	1180.8311	-8	R(17)	1182.0362	-1	R(18)	1183.2299	-2	R(20)	1185.5865	2	R(21)	1186.7488	0
R(22)	1187.9002	-4	R(23)	1189.0417	-1	R(24)	1190.1723	-2	R(25)	1191.2927	2	R(26)	1192.4021	1
R(30)	1196.7328	1	R(31)	1197.7887	1	R(32)	1198.8342	6	R(33)	1199.8678	0	R(34)	1200.8896	-16
R(35)	1201.9036	-1	R(36)	1202.9059	5	R(38)	1204.8755	-4	R(39)	1205.8445	-2	R(40)	1206.8032	6
R(42)	1208.6858	6	R(43)	1209.6113	14	R(44)	1210.5239	4	R(45)	1211.4262	1	R(47)	1213.1970	-8
R(48)	1214.0670	2	R(49)	1214.9264	18	R(50)	1215.7709	-4	R(51)	1216.6081	15	R(52)	1217.4306	-1
R(53)	1218.2427	-7	R(55)	1219.8353	4	R(56)	1220.6177	42	R(57)	1221.3808	-1	R(58)	1222.1389	22
R(59)	1222.8808	-2	R(60)	1223.6145	6	R(63)	1225.7445	12	R(64)	1226.4297	-3	R(65)	1227.1042	-8
R(66)	1227.7638	-46	R(68)	1229.0608	5									
(8, 7) Band														
P(107)	947.6974	13	P(105)	952.3017	-2	P(102)	959.1542	7	P(100)	963.6832	3	P(98)	968.1779	-34
P(97)	970.4186	-4	P(96)	972.6500	12	P(94)	977.0851	1	P(93)	979.2922	8	P(92)	981.4896	-4
P(90)	985.8637	5	P(89)	988.0384	4	P(88)	990.2049	1	P(87)	992.3651	14	P(86)	994.5158	12
P(85)	996.6575	1	P(84)	998.7953	31	P(81)	1005.1484	3	P(79)	1009.3452	4	P(77)	1013.5087	-1
P(73)	1021.7386	6	P(68)	1031.8372	-2	P(57)	1053.3131	16	P(55)	1057.1039	-1	P(52)	1062.7271	-5
P(51)	1064.5844	-1	P(50)	1066.4326	-1	P(49)	1068.2706	-14	P(48)	1070.1023	-3	P(47)	1071.9248	6
P(46)	1073.7369	0	P(44)	1077.3361	5	P(43)	1079.1209	-5	P(42)	1080.8964	-19	P(40)	1084.4255	4
P(39)	1086.1761	12	P(38)	1087.9154	-2	P(36)	1091.3699	3	P(35)	1093.0817	-13	P(34)	1094.7855	-17
P(33)	1096.4829	7	P(32)	1098.1696	17	P(30)	1101.5106	-10	P(29)	1103.1722	27	P(28)	1104.8181	0
P(27)	1106.4573	-1	P(26)	1108.0861	-13	P(25)	1109.7074	-5	P(23)	1112.9207	0	P(22)	1114.5128	-1
P(21)	1116.0950	-7	P(19)	1119.2336	9	P(17)	1122.3310	-4	P(16)	1123.8650	-14	P(15)	1125.3918	0
P(14)	1126.9079	3	P(13)	1128.4121	-15	P(12)	1129.9106	6	P(10)	1132.8751	16	P(6)	1138.6840	6
R(2)	1151.1770	8	R(5)	1155.1610	11	R(6)	1156.4670	-6	R(7)	1157.7665	14	R(8)	1159.0532	8
R(9)	1160.3313	18	R(10)	1161.5964	1	R(11)	1162.8526	-2	R(12)	1164.0997	5	R(15)	1167.7765	5
R(17)	1170.1756	4	R(19)	1172.5329	1	R(21)	1174.8499	15	R(25)	1179.3513	-15	R(26)	1180.4518	-7
R(27)	1181.5409	-6	R(34)	1188.8634	-1	R(36)	1190.8578	-4	R(37)	1191.8409	16	R(39)	1193.7683	-1
R(40)	1194.7165	-1	R(41)	1195.6542	5	R(42)	1196.5798	0	R(43)	1197.4944	-4	R(44)	1198.3991	3
R(45)	1199.2912	-4	R(48)	1201.9036	2	R(49)	1202.7514	-2	R(50)	1203.5858	0	R(51)	1204.4147	5
R(52)	1205.2288	2	R(53)	1206.0317	0	R(55)	1207.6028	-12	R(56)	1208.3730	0	R(58)	1209.8768	-1
R(59)	1210.6117	1	R(62)	1212.7465	-4	R(63)	1213.4356	0	R(64)	1214.1131	4	R(67)	1216.0737	-5
R(68)	1216.7044	-2	R(69)	1217.3236	1	R(70)	1217.9297	-8	R(72)	1219.1109	17	R(78)	1222.3649	39
R(79)	1222.8623	10	R(80)	1223.3495	1	R(81)	1223.8238	-19	R(82)	1224.2899	1	R(83)	1224.7397	-21
(9, 8) Band														
P(107)	937.1594	-13	P(104)	944.0249	-9	P(102)	948.5640	-5	P(101)	950.8223	-1	P(100)	953.0727	2
P(99)	955.3147	-2	P(98)	957.5457	-40	P(97)	959.7761	-6	P(94)	966.4085	-22	P(93)	968.6072	8
P(90)	975.1471	8	P(88)	979.4664	-2	P(86)	983.7574	24	P(85)	985.8873	0	P(84)	988.0116	1
P(83)	990.1269	-7	P(82)	992.2342	-14	P(81)	994.3338	-18	P(80)	996.4266	-8	P(79)	998.5099	-12
P(78)	1000.5868	2	P(77)	1002.6538	-1	P(72)	1012.8692	22	P(71)	1014.8853	7	P(70)	1016.8974	34
P(69)	1018.8967	17	P(64)	1028.7736	-2	P(63)	1030.7239	-3	P(56)	1044.1370	3	P(53)	1049.7553	1
P(50)	1055.2934	-14	P(49)	1057.1217	-20	P(48)	1058.9412	-27	P(47)	1060.7536	-15	P(43)	1067.9103	-7
P(42)	1069.6775	0	P(41)	1071.4361	10	P(40)	1073.1848	12	P(38)	1076.6515	-21	P(37)	1078.3746	-2
P(35)	1081.7909	8	P(33)	1085.1683	-4	P(32)	1086.8443	2	P(31)	1088.5101	-3	P(29)	1091.8169	18
P(28)	1093.4536	1	P(27)	1095.0832	7	P(26)	1096.7032	9	P(25)	1098.3125	-1	P(24)	1099.9135	0
P(22)	1103.0871	0	P(21)	1104.6589	-8	P(19)	1107.7763	-1	P(17)	1110.8540	-8	P(16)	1112.3807	10
P(15)	1113.8957	7	P(11)	1119.8600	6	P(9)	1122.7829	-4	P(7)	1125.6692	12	P(6)	1127.0969	12
P(5)	1128.5149	13	R(14)	1154.7624	-14	R(15)	1155.9690	-2	R(16)	1157.1640	-2	R(17)	1158.3486	-1
R(20)	1161.8399	1	R(21)	1162.9828	4	R(22)	1164.1146	0	R(23)	1165.2376	13	R(24)	1166.3463	-9
R(28)	1170.6853	1	R(30)	1172.7903	4	R(32)	1174.8499	-19	R(35)	1177.8615	-19	R(36)	1178.8441	-15
R(37)	1179.8169	0	R(39)	1181.7264	-2	R(41)	1183.5923	-1	R(42)	1184.5086	-3	R(48)	1189.7765	22

TABLE 2—Continued

Line	Observed	δ	Line	Observed	δ	Line	Observed	δ	Line	Observed	δ	Line	Observed	δ
$^{28}\text{Si}^{16}\text{O}$														
(9, 8) Band														
R(49)	1190.6127	-2	R(51)	1192.2556	-6	R(53)	1193.8556	11	R(54)	1194.6365	-1	R(55)	1195.4080	6
R(56)	1196.1667	-2	R(57)	1196.9149	1	R(58)	1197.6515	0	R(59)	1198.3772	6	R(63)	1201.1617	-4
R(65)	1202.4844	-10	R(66)	1203.1296	-1	R(67)	1203.7620	-3	R(68)	1204.3856	24	R(69)	1204.9953	29
R(71)	1206.1750	-5	R(72)	1206.7494	-1	R(73)	1207.3107	-9	R(77)	1209.4406	-6	R(78)	1209.9429	-9
(10, 9) Band														
P(95)	953.5766	11	P(92)	960.1317	9	P(91)	962.3011	9	P(90)	964.4611	-5	P(89)	966.6148	-3
P(88)	968.7601	-7	P(87)	970.8991	8	P(86)	973.0293	13	P(85)	975.1471	-25	P(84)	977.2645	13
P(83)	979.3722	34	P(82)	981.4670	8	P(81)	983.5527	-29	P(80)	985.6363	-6	P(76)	993.8826	23
P(75)	995.9224	17	P(74)	997.9536	9	P(73)	999.9767	2	P(72)	1001.9937	16	P(71)	1003.9998	5
P(69)	1007.9871	-16	P(61)	1023.6091	-1	P(58)	1029.3261	-2	P(57)	1031.2146	-1	P(56)	1033.0945	1
P(51)	1042.3634	5	P(50)	1044.1890	-12	P(43)	1056.7341	1	P(40)	1061.9747	-11	P(39)	1063.7051	1
P(35)	1070.5324	16	P(28)	1082.1227	1	P(27)	1083.7419	4	P(24)	1088.5420	0	P(23)	1090.1236	4
P(22)	1091.6952	1	P(19)	1096.3554	15	P(18)	1097.8870	-9	P(17)	1099.4125	3	P(16)	1100.9266	-3
P(15)	1102.4325	4	P(14)	1103.9282	6	P(13)	1105.4143	9	P(10)	1109.8133	4	P(8)	1112.6996	24
R(6)	1133.0671	4	R(7)	1134.3432	-11	R(9)	1136.8682	-8	R(10)	1138.1158	-1	R(11)	1139.3534	7
R(13)	1141.7919	-35	R(15)	1144.1969	3	R(17)	1146.5586	21	R(19)	1148.8750	4	R(21)	1151.1507	-1
R(24)	1154.4861	0	R(26)	1156.6570	3	R(27)	1157.7265	4	R(28)	1158.7853	6	R(31)	1161.9020	55
R(33)	1163.9175	3	R(34)	1164.9113	0	R(37)	1167.8295	8	R(38)	1168.7018	-775	R(39)	1169.7187	-2
R(40)	1170.6479	3	R(41)	1171.5639	-14	R(42)	1172.4721	1	R(43)	1173.3661	-15	R(45)	1175.1257	0
R(48)	1177.6799	5	R(50)	1179.3252	-7	R(51)	1180.1311	-11	R(53)	1181.7112	0	R(55)	1183.2446	-2
R(56)	1183.9950	4	R(58)	1185.4597	-3	R(61)	1187.5718	-3	R(64)	1189.5789	-15	R(65)	1190.2262	-4
R(68)	1192.0950	-6	R(69)	1192.6945	-6									
(11,10) Band														
P(92)	949.4989	-2	P(90)	953.8088	-1	P(89)	955.9517	-1	P(87)	960.2142	3	P(86)	962.3311	-19
P(85)	964.4448	8	P(84)	966.5481	10	P(82)	970.7285	-5	P(79)	976.9403	-9	P(78)	978.9963	6
P(76)	983.0802	2	P(75)	985.1101	3	P(74)	987.1314	-1	P(73)	989.1450	2	P(72)	991.1523	25
P(70)	995.1357	7	P(69)	997.1161	11	P(68)	999.0867	0	P(67)	1001.0483	-17	P(66)	1003.0051	3
P(64)	1006.8888	-4	P(60)	1014.5568	9	P(59)	1016.4501	-10	P(55)	1023.9455	-4	P(53)	1027.6425	11
P(44)	1043.8354	0	P(43)	1045.5899	-4	P(42)	1047.3347	-16	P(39)	1052.5206	5	P(36)	1057.6212	-13
P(29)	1069.2065	-8	P(26)	1074.0327	-7	P(25)	1075.6217	-16	P(23)	1078.7744	-7	P(22)	1080.3364	-4
P(20)	1083.4317	-2	P(18)	1086.4906	17	P(17)	1088.0046	14	P(13)	1093.9656	15	P(11)	1096.8859	-7
P(10)	1098.3324	-10	P(8)	1101.1972	-3	P(7)	1102.6141	-8	P(6)	1104.0209	-16	R(9)	1125.1908	11
R(12)	1128.8702	0	R(13)	1130.0754	-11	R(14)	1131.2719	-5	R(17)	1134.7976	-5	R(18)	1135.9531	6
R(20)	1138.2296	-4	R(21)	1139.3534	4	R(23)	1141.5699	24	R(24)	1142.6597	8	R(25)	1143.7398	1
R(27)	1145.8694	0	R(28)	1146.9212	29	R(29)	1147.9566	1	R(33)	1152.0038	19	R(34)	1152.9864	1
R(37)	1155.8737	-6	R(38)	1156.8164	13	R(39)	1157.7478	26	R(40)	1158.6639	-1	R(41)	1159.5720	-1
R(44)	1162.2283	-16	R(45)	1163.0936	0	R(46)	1163.9458	-5	R(48)	1165.6179	-3	R(51)	1168.0427	7
R(53)	1169.6004	-12	R(56)	1171.8567	7	R(58)	1173.3029	8	R(59)	1174.0087	7	R(61)	1175.3852	-1
R(63)	1176.7164	0	R(64)	1177.3647	0	R(65)	1178.0000	-14	R(67)	1179.2399	2	R(68)	1179.8387	-27
R(69)	1180.4312	-1	R(70)	1181.0087	-9	R(71)	1181.5765	4	R(75)	1183.7218	-21	R(79)	1185.6820	5
(12,11) Band														
P(87)	949.5598	-14	P(84)	955.8636	7	P(82)	960.0218	-19	P(81)	962.0893	-28	P(77)	970.2849	7
P(74)	976.3433	10	P(73)	978.3457	5	P(72)	980.3394	-3	P(71)	982.3259	-2	P(70)	984.3036	-4
P(61)	1001.7232	-41	P(57)	1009.2501	4	P(55)	1012.9578	-13	P(54)	1014.8018	10	P(53)	1016.6337	0
P(52)	1018.4595	15	P(48)	1025.6672	-1	P(46)	1029.2161	-28	P(29)	1057.9522	-12	P(26)	1062.7477	-12
P(25)	1064.3335	48	P(23)	1067.4606	4	P(22)	1069.0110	-8	P(21)	1070.5543	4	P(20)	1072.0841	-26
P(18)	1075.1227	-8	P(14)	1081.0799	-26	P(13)	1082.5477	-5	P(12)	1084.0045	3	P(11)	1085.4509	3
R(11)	1115.9902	20	R(14)	1119.5782	9	R(20)	1126.4757	-1	R(23)	1129.7853	16	R(29)	1136.1120	-19
R(31)	1138.1385	-1	R(33)	1140.1263	61	R(38)	1144.8844	-3	R(39)	1145.8088	39	R(41)	1147.6150	26

TABLE 2—Continued

Line	Observed	δ	Line	Observed	δ	Line	Observed	δ	Line	Observed	δ	Line	Observed	δ
$^{28}\text{Si}^{16}\text{O}$														
(12,11) Band														
R(44)	1150.2408	-2	R(45)	1151.0994	44	R(46)	1151.9394	14	R(48)	1153.5903	-2	R(50)	1155.1984	1
R(52)	1156.7592	-18	R(53)	1157.5200	-55	R(54)	1158.2814	27	R(58)	1161.1772	-5	R(59)	1161.8712	-27
R(60)	1162.5583	-3	R(61)	1163.2297	-21	R(64)	1165.1828	6	R(65)	1165.8092	0	R(68)	1167.6210	6
R(71)	1169.3252	-9	R(72)	1169.8709	-4	R(73)	1170.4030	-15						
(13,12) Band														
P(73)	967.5808	32	P(66)	981.2935	19	P(60)	992.7164	-16	P(59)	994.5930	4	P(56)	1000.1698	52
P(55)	1002.0053	7	P(52)	1007.4731	5	P(51)	1009.2781	4	P(49)	1012.8656	38	P(45)	1019.9237	-3
P(37)	1033.6174	-18	P(35)	1036.9484	-41	P(24)	1054.6298	23	P(19)	1062.2895	20	P(18)	1063.7969	57
P(12)	1072.6142	28	P(11)	1074.0547	69	P(10)	1075.4744	0	P(9)	1076.8901	-12	P(7)	1079.6959	1
R(8)	1100.7071	28	R(12)	1105.5545	16	R(15)	1109.0816	2	R(19)	1113.6387	-23	R(21)	1115.8585	4
R(28)	1123.2857	-3	R(30)	1125.3135	10	R(39)	1133.8980	1	R(40)	1134.7976	1	R(42)	1136.5617	-17
R(45)	1139.1358	61	R(48)	1141.5940	-20	R(51)	1143.9581	-36	R(53)	1145.4818	-7	R(54)	1146.2259	-1
R(56)	1147.6788	-1	R(59)	1149.7722	-5	R(60)	1150.4480	2	R(62)	1151.7623	-10	R(66)	1154.2565	7
R(68)	1155.4321	-2												
$^{29}\text{Si}^{16}\text{O}$														
(1, 0) Band														
P(96)	1042.9914	-12	P(85)	1067.4713	4	P(84)	1069.6491	1	P(83)	1071.8202	11	P(81)	1076.1380	27
P(79)	1080.4189	-4	P(78)	1082.5478	-15	P(77)	1084.6710	-1	P(74)	1090.9868	-9	P(70)	1099.2944	-7
P(69)	1101.3515	2	P(68)	1103.3984	-8	P(67)	1105.4402	13	P(65)	1109.4927	-3	P(60)	1119.4825	13
P(57)	1125.3717	-6	P(56)	1127.3174	-15	P(54)	1131.1853	-9	P(53)	1133.1067	-2	P(50)	1138.8177	5
P(49)	1140.7016	-15	P(48)	1142.5785	-19	P(46)	1146.3072	-13	P(44)	1150.0034	21	P(42)	1153.6580	-7
P(39)	1159.0781	1	P(37)	1162.6456	-4	P(36)	1164.4160	-4	P(35)	1166.1773	-5	P(31)	1173.1323	-3
P(27)	1179.9411	3	P(26)	1181.6197	-1	P(25)	1183.2894	-1	P(23)	1186.6002	-8	P(22)	1188.2420	-7
P(17)	1196.3112	7	P(16)	1197.8953	-4	P(13)	1202.5946	4	P(12)	1204.1441	29	P(10)	1207.2054	-10
P(8)	1210.2334	3	P(7)	1211.7323	4	P(6)	1213.2243	33	P(3)	1217.6338	41			
(2, 1) Band														
P(107)	1006.9427	-15	P(103)	1016.2459	-18	P(98)	1027.7058	-12	P(80)	1067.3533	-21	P(79)	1069.4824	-4
P(78)	1071.6029	8	P(77)	1073.7137	3	P(76)	1075.8137	-29	P(75)	1077.9096	-19	P(74)	1079.9982	-2
P(73)	1082.0773	3	P(72)	1084.1458	-17	P(71)	1086.2084	-13	P(70)	1088.2622	-15	P(69)	1090.3104	10
P(68)	1092.3476	8	P(66)	1096.3964	-3	P(65)	1098.4083	-8	P(64)	1100.4123	-8	P(63)	1102.4090	3
P(60)	1108.3446	-4	P(59)	1110.3067	-2	P(58)	1112.2599	-2	P(57)	1114.2037	-12	P(56)	1116.1401	-10
P(54)	1119.9870	-6	P(52)	1123.7989	-8	P(51)	1125.6930	2	P(49)	1129.4518	-10	P(48)	1131.3192	-5
P(47)	1133.1779	1	P(45)	1136.8682	5	P(44)	1138.6984	-10	P(43)	1140.5227	4	P(42)	1142.3358	-5
P(41)	1144.1415	1	P(37)	1151.2741	18	P(36)	1153.0321	-4	P(35)	1154.7840	2	P(34)	1156.5253	-6
P(33)	1158.2587	-2	P(32)	1159.9820	-9	P(31)	1161.6979	2	P(28)	1166.7873	1	P(27)	1168.4653	0
P(26)	1170.1343	1	P(25)	1171.7927	-11	P(24)	1173.4441	0	P(23)	1175.0839	-12	P(22)	1176.7163	-4
P(21)	1178.3386	-5	P(20)	1179.9525	5	P(19)	1181.5555	0	P(18)	1183.1456	-40	P(15)	1187.8742	-8
P(12)	1192.5133	-15	P(11)	1194.0415	-8	P(10)	1195.5597	-4	P(7)	1200.0567	9	P(4)	1204.4591	-50
R(4)	1217.1569	-16	R(7)	1221.2105	-6	R(8)	1222.5416	-3	R(9)	1223.8618	-9	R(13)	1229.0448	6
R(15)	1231.5748	9	R(18)	1235.2911	-5	R(19)	1236.5119	16						
(3, 2) Band														
P(84)	1047.9148	-10	P(79)	1058.5739	-64	P(77)	1062.7881	-17	P(74)	1069.0429	-3	P(73)	1071.1126	13
P(72)	1073.1693	-19	P(71)	1075.2222	-8	P(70)	1077.2630	-34	P(69)	1079.3012	-4	P(67)	1083.3475	3
P(65)	1087.3592	-3	P(63)	1091.3380	-3	P(62)	1093.3141	-10	P(61)	1095.2831	-3	P(59)	1099.1954	7
P(58)	1101.1371	-5	P(57)	1103.0709	-10	P(56)	1104.9960	-18	P(55)	1106.9142	-8	P(54)	1108.8237	1
P(53)	1110.7233	-4	P(51)	1114.4979	1	P(50)	1116.3712	-6	P(49)	1118.2359	-12	P(48)	1120.0920	-17
P(47)	1121.9410	-5	P(45)	1125.6108	0	P(44)	1127.4321	-2	P(42)	1131.0489	2	P(41)	1132.8420	-15

TABLE 2—Continued

Line	Observed	δ	Line	Observed	δ	Line	Observed	δ	Line	Observed	δ	Line	Observed	δ
$^{29}\text{Si}^{16}\text{O}$														
(3, 2) Band														
P(39)	1136.4070	6	P(38)	1138.1765	20	P(37)	1139.9349	14	P(36)	1141.6832	-3	P(34)	1145.1577	12
P(33)	1146.8802	8	P(32)	1148.5953	21	P(30)	1151.9940	6	P(29)	1153.6781	-17	P(28)	1155.3564	-6
P(26)	1158.6835	-2	P(25)	1160.3314	-18	P(24)	1161.9729	-6	P(23)	1163.6046	2	P(20)	1168.4393	-17
P(19)	1170.0330	-15	P(10)	1183.9482	-10	P(7)	1188.4149	-1	P(3)	1194.2333	-2	R(5)	1206.7494	-9
R(6)	1208.0917	3	R(7)	1209.4241	16	R(8)	1210.7433	-1	R(10)	1213.3544	-8	R(11)	1214.6260	-199
R(12)	1215.9253	-12	R(16)	1220.9488	18	R(17)	1222.1763	-2	R(18)	1223.3966	8	R(19)	1224.6039	-8
R(20)	1225.8007	-26												
(4, 3) Band														
P(79)	1047.7054	-60	P(72)	1062.2306	18	P(69)	1068.3262	-16	P(67)	1072.3496	-30	P(66)	1074.3512	-12
P(65)	1076.3432	-8	P(64)	1078.3274	2	P(62)	1082.2680	-3	P(61)	1084.2263	0	P(59)	1088.1161	-7
P(53)	1099.5831	-5	P(52)	1101.4647	0	P(49)	1107.0548	-10	P(48)	1108.9013	-9	P(47)	1110.7392	-5
P(46)	1112.5675	-9	P(44)	1116.1989	-8	P(40)	1123.3558	0	P(35)	1132.0996	-4	P(31)	1138.9320	-8
P(30)	1140.6197	15	P(27)	1145.6192	-1	P(25)	1148.9063	-12	P(24)	1150.5366	-9	P(23)	1152.1583	-1
P(21)	1155.3716	-5	P(18)	1160.1224	-1	P(16)	1163.2423	1	P(15)	1164.7872	-6	P(13)	1167.8516	9
P(12)	1169.3676	-2	P(10)	1172.3701	-31	P(9)	1173.8596	-19	P(7)	1176.8083	-9	P(6)	1178.2682	-3
R(4)	1193.6775	24	R(11)	1202.8541	7	R(12)	1204.1226	-16	R(13)	1205.3856	7	R(16)	1209.1052	-6
R(18)	1211.5325	-27	R(20)	1213.9241	7	R(27)	1221.9559	8	R(32)	1227.3757	-15			
(5, 4) Band														
P(84)	1026.3139	-29	P(83)	1028.4451	5	P(76)	1043.1139	-11	P(62)	1071.2550	-4	P(61)	1073.2024	-5
P(58)	1078.9942	-6	P(54)	1086.5979	-3	P(50)	1094.0646	7	P(49)	1095.9082	-5	P(48)	1097.7442	-5
P(47)	1099.5715	-5	P(42)	1108.5759	-7	P(40)	1112.1161	-5	P(39)	1113.8710	-22	P(37)	1117.3577	-18
P(35)	1120.8089	-10	P(31)	1127.6023	2	P(29)	1130.9386	-49	P(27)	1134.2481	-2	P(23)	1140.7481	10
P(21)	1143.9405	-2	P(16)	1151.7622	15	P(15)	1153.2949	-15	P(11)	1159.3434	-6	R(5)	1183.3169	-5
R(6)	1184.6390	1	R(7)	1185.9513	9	R(11)	1191.0956	-2	R(17)	1198.5098	1	R(28)	1211.1369	-17
R(30)	1213.2976	-13	R(32)	1215.4151	-18	R(33)	1216.4600	1	R(34)	1217.4923	0	R(38)	1221.5138	-13
R(41)	1224.4197	5	R(44)	1227.2275	16									
(6, 5) Band														
P(61)	1062.2119	-13	P(58)	1067.9722	-20	P(57)	1069.8780	5	P(56)	1071.7721	-3	P(55)	1073.6583	-3
P(51)	1081.1154	-23	P(45)	1092.0456	-5	P(44)	1093.8375	6	P(43)	1095.6170	-17	P(40)	1100.9117	4
P(39)	1102.6582	4	P(35)	1109.5539	0	P(27)	1122.9110	-5	P(24)	1127.7671	-22	P(13)	1144.8626	3
R(14)	1183.0955	-9	R(22)	1192.5762	-2	R(29)	1200.3262	-9	R(31)	1202.4471	0	R(35)	1206.5603	5
R(37)	1208.5509	-12	R(42)	1213.3434	-12	R(44)	1215.1862	3						
$^{30}\text{Si}^{16}\text{O}$														
(1, 0) Band														
P(92)	1047.0359	-12	P(87)	1057.9718	-15	P(83)	1066.5819	-6	P(82)	1068.7147	-4	P(78)	1077.1661	-9
P(72)	1089.6038	-13	P(71)	1091.6494	-6	P(70)	1093.6849	-18	P(68)	1097.7340	-17	P(67)	1099.7456	-23
P(65)	1103.7482	4	P(62)	1109.6863	8	P(61)	1111.6477	-5	P(59)	1115.5456	-29	P(57)	1119.4150	-3
P(55)	1123.2477	-7	P(54)	1125.1512	-10	P(53)	1127.0480	4	P(51)	1130.8119	-9	P(50)	1132.6808	-17
P(46)	1140.0745	-10	P(44)	1143.7191	-11	P(41)	1149.1206	-11	P(40)	1150.9032	-14	P(39)	1152.6774	-14
P(38)	1154.4429	-13	P(34)	1161.4179	10	P(32)	1164.8457	-41	P(30)	1168.2466	-1	P(29)	1169.9315	-1
P(28)	1171.6067	-8	P(26)	1174.9305	-16	P(24)	1178.2236	34	P(22)	1181.4708	-9	P(20)	1184.6860	-3
P(19)	1186.2789	-9	P(15)	1192.5587	-19	P(12)	1197.1747	16	P(8)	1203.1929	20			
(2, 1) Band														
P(76)	1070.5008	-9	P(72)	1078.7187	-16	P(71)	1080.7536	-13	P(69)	1084.7971	-24	P(65)	1092.7904	-3

TABLE 2—Continued

Line	Observed	δ	Line	Observed	δ	Line	Observed	δ	Line	Observed	δ	Line	Observed	δ
$^{30}\text{Si}^{16}\text{O}$														
(2, 1) Band														
P(64)	1094.7668	-12	P(63)	1096.7353	-17	P(60)	1102.5936	-6	P(57)	1108.3754	-9	P(56)	1110.2855	-13
P(55)	1112.1878	-12	P(54)	1114.0805	-21	P(53)	1115.9678	1	P(48)	1125.2645	-11	P(47)	1127.0969	-26
P(45)	1130.7405	-7	P(44)	1132.5471	-19	P(42)	1136.1379	-8	P(40)	1139.6898	-34	P(39)	1141.4559	-14
P(38)	1143.2123	-4	P(36)	1146.6954	-13	P(35)	1148.4258	4	P(34)	1150.1458	5	P(31)	1155.2497	-14
P(30)	1156.9342	-8	P(16)	1179.5564	25	P(15)	1181.1037	33	P(13)	1184.1641	-9	P(12)	1185.6819	-15
P(5)	1196.0451	-11	P(3)	1198.9235	24	R(5)	1211.3785	-7	R(7)	1214.0400	-1			
(3, 2) Band														
P(78)	1055.5552	2	P(74)	1063.7988	24	P(71)	1069.8927	-5	P(70)	1071.9070	-23	P(66)	1079.8916	-5
P(64)	1083.8337	-7	P(63)	1085.7932	0	P(59)	1093.5435	-17	P(58)	1095.4621	-3	P(57)	1097.3697	-14
P(56)	1099.2733	18	P(55)	1101.1618	-16	P(51)	1108.6452	-13	P(50)	1110.4978	19	P(49)	1112.3385	17
P(48)	1114.1678	-13	P(47)	1115.9903	-25	P(45)	1119.6119	-24	P(42)	1124.9795	-20	P(41)	1126.7521	-11
P(40)	1128.5148	-12	P(39)	1130.2682	-18	P(37)	1133.7497	-21	P(34)	1138.9064	-14	P(30)	1145.6561	-16
P(25)	1153.8914	-9	P(23)	1157.1217	-7	P(22)	1158.7230	-8	P(19)	1163.4718	-8	P(17)	1166.5915	-7
P(13)	1172.7202	5	P(9)	1178.6966	-5	R(6)	1201.0723	-26	R(7)	1202.3901	-8	R(12)	1208.8221	1
(4, 3) Band														
P(84)	1032.2593	-13	P(79)	1042.7291	3	P(68)	1065.0585	5	P(67)	1067.0387	-6	P(65)	1070.9767	-9
P(62)	1076.8223	-8	P(53)	1093.9083	-15	P(49)	1101.2828	-14	P(48)	1103.1052	-12	P(45)	1108.5209	-5
P(43)	1112.0874	-6	P(42)	1113.8584	1	P(40)	1117.3726	-1	P(34)	1127.7046	0	P(33)	1129.3944	-11
P(31)	1132.7492	-14	P(29)	1136.0688	-9	P(27)	1139.3535	7	P(26)	1140.9801	-6	P(25)	1142.5997	2
P(24)	1144.2093	0	P(20)	1150.5560	-7	P(19)	1152.1195	-11	P(12)	1162.8067	-8	P(11)	1164.2961	-7
P(8)	1168.7080	0	R(5)	1188.1531	-7	R(6)	1189.4687	-12	R(17)	1203.2924	-8	R(22)	1209.1736	-12
R(26)	1213.6954	-11												
(5, 4) Band														
P(58)	1073.5723	-8	P(57)	1075.4614	-1	P(53)	1082.9307	-4	P(47)	1093.8776	-31	P(46)	1095.6767	10
P(43)	1101.0069	-16	P(42)	1102.7683	-5	P(39)	1107.9970	-2	P(37)	1111.4370	-18	P(36)	1113.1463	-2
P(34)	1116.5345	-6	P(32)	1119.8873	-8	P(27)	1128.1132	-6	P(22)	1136.1121	-8	P(20)	1139.2457	-29
P(16)	1145.4079	-13	P(13)	1149.9304	-16	P(11)	1152.9004	0	P(9)	1155.8302	-9	R(19)	1193.9804	-9
R(22)	1197.4507	-6	R(26)	1201.9340	-12	R(27)	1203.0305	-1	R(37)	1213.4122	-4			
(6, 5) Band														
P(52)	1073.8213	-5	P(51)	1075.6484	-11	P(45)	1086.4350	-9	P(40)	1095.1863	-7	P(39)	1096.9105	-6
P(38)	1098.6251	-13	P(34)	1105.3977	-15	P(31)	1110.3845	-9	P(26)	1118.5157	-8	P(23)	1123.2859	-6
R(11)	1172.6981	-11	R(17)	1179.9745	-7	R(19)	1182.3249	46	R(42)	1206.3311	-11	R(48)	1211.6769	-39

^a Observed – calculated residuals (δ) are in units of 0.0001 cm⁻¹.

tion on the silicon center; none of the Δ_{ij}^{Si} parameters were statistically well determined.

In Table 5 we compare our calculated Dunham Y_{ij} constants for ^{28}SiO , ^{29}SiO , and ^{30}SiO , which were obtained by multiplying the U_{ij} 's in Table 4 by the reduced mass factor $\mu^{-(i+2j)/2}$, to those reported by Glenar et al. (1985). Comparing the listed uncertainties alone indicates considerable improvement in the $X^1\Sigma$ molecular constants.

3.2. Modified-Morse Internuclear Potential

In the second global fit a different procedure was tried that involved fitting the data directly to the numerical eigenvalues of the radial Schrödinger equation,

$$\left\{ \frac{\hbar^2}{2\mu} \nabla^2 - U^{\text{eff}}(R) + E(v, J) - \frac{\hbar^2}{2\mu} [1 + q(R)] J(J+1)/R^2 \right\} \times \psi(r; v, J) = 0, \quad (5)$$

using an effective internuclear potential,

$$U^{\text{eff}}(R) = U^{\text{BO}}(R) + U^{\text{C}}(R), \quad (6)$$

where the modified-Morse function,

$$U^{\text{BO}} = D_e \{1 - \exp[-\beta(R)]\}^2 / \{1 - \exp[-\beta(\infty)]\}^2, \quad (7)$$

TABLE 3
SiO PURE ROTATIONAL LINES^a

v	J	ν	δ	Ref. ^b	v	J	ν	δ	Ref. ^b	v	J	ν	δ	Ref. ^b
²⁸ Si ¹⁶ O														
0	0	1.4484607	-30	A	2	6	9.9970463	2	C	10	5	8.0883991	7	C
0	1	2.8969028	-7	B	2	7	11.4247165	-4	C	10	7	10.7836334	6	C
0	2	4.3452931	-23	B	3	0	1.4182925	-13	A	11	5	8.0285110	10	C
0	3	5.7936184	28	B	3	3	5.6729362	3	B	11	7	10.7037816	9	C
0	4	7.2418426	24	B	3	4	7.0909923	20	B	13	5	7.9088548	8	C
0	5	8.6899458	5	B	3	5	8.5089251	2	C	13	6	9.2266306	3	C
0	6	10.1379067	0	B	3	7	11.3443392	0	C	13	7	10.5442380	4	C
0	7	11.5857006	-4	C	4	4	7.0407999	-8	B	14	5	7.8490827	2	C
1	0	1.4383961	-14	A	4	5	8.4486975	5	C	14	6	9.1568969	4	C
1	1	2.8767692	-18	B	4	6	9.8564505	4	C	14	7	10.4645413	0	C
1	2	4.3150932	-34	B	4	7	11.2640355	4	C	15	5	7.7893458	0	C
1	3	5.7533519	13	B	5	6	9.7862475	7	C	15	7	10.3848912	-1	C
1	4	7.1915068	-20	B	5	7	11.1838030	4	C	16	5	7.7296413	-5	C
1	5	8.6295517	42	C	6	5	8.3284014	2	C	16	6	9.0175470	-10	C
1	5	8.6295475	0	B	6	6	9.7161052	10	C	16	7	10.3052840	-9	C
1	6	10.0674425	0	C	6	7	11.036397	4	C	17	5	7.6699670	-11	C
1	7	11.5051676	-26	C	7	6	9.6460210	7	C	17	7	10.2257170	-18	C
2	0	1.4283375	-35	A	8	6	9.5759937	7	C	18	5	7.6103208	-16	C
2	1	2.8566583	4	B	8	7	10.9435124	9	C	18	7	10.1461879	-21	C
2	3	5.7131284	41	B	9	5	8.1483308	9	C	19	6	8.8087813	-29	C
2	4	7.1412250	-9	B	9	6	9.5060214	12	C	19	7	10.0666928	-28	C
²⁹ Si ¹⁶ O					0 0 1.4303168 -29 A					³⁰ Si ¹⁶ O				
0 0 1.4134225 -4 A														

^a Observed – calculated (δ) are in units of 10^{-7} cm⁻¹^b A: Törring 1968; B: Manson et al. 1977; C: Mollaaghataba et al. 1991.

TABLE 4
MASS-REDUCED DUNHAM CONSTANTS^a

U_{10}	3960.64332(17)
U_{20}	-60.800711(198)
U_{30}	0.1981766(801)
$10^3 U_{40}$	-1.1999(104)
U_{01}	7.39594491(39)
U_{11}	-0.163559749(306)
$10^4 U_{21}$	2.60404(193)
$10^6 U_{31}$	-6.2345(379)
$10^7 U_{41}$	-2.0125(212)
$10^4 U_{02}$	-1.03159571
$10^7 U_{12}$	-1.36508752
$10^8 U_{22}$	-1.95757118
$10^{10} U_{32}$	-8.55123928
$10^{11} U_{03}$	3.76958577
$10^{11} U_{13}$	-2.66817826
$10^{12} U_{23}$	-1.32301772
$10^{14} U_{33}$	-4.74899470
$10^{14} U_{04}$	-1.12355313
$10^{15} U_{14}$	-1.08769417
$10^{17} U_{24}$	-8.70050397
$10^{19} U_{05}$	-2.46507359
$10^{20} U_{15}$	-4.84767956
$10^{21} U_{25}$	-3.765633782
$10^{24} U_{06}$	-9.88789619
$10^{24} U_{16}$	-2.45591146
$10^{28} U_{07}$	-3.78229842
$10^{28} U_{17}$	-1.06468002
$10^{32} U_{08}$	-1.62442346
$10^{37} U_{09}$	-6.96563341
μ (²⁸ Si ¹⁶ O) (u)	10.17670725
μ (²⁹ Si ¹⁶ O) (u)	10.30602703
μ (³⁰ Si ¹⁶ O) (u)	10.42944561

^a In units of cm⁻¹. Uncertainties (numbers in parentheses) are quoted to 1σ . Standard deviation of the fit was 0.8579 involving 2186 rotational lines in the range, $0 \leq v \leq 40$.

was used to represent the Born-Oppenheimer potential where

$$\beta(R) = z \sum_{i=0} \beta_i z^i, \quad (8)$$

$$z = (R - R_e)/(R + R_e). \quad (9)$$

Corrections for breakdown in the Born-Oppenheimer approximation are represented by power series expansions where

$$U^C(R) = M_A^{-1} \sum_{i=1} u_i^A (R - R_e)^i + M_B^{-1} \sum_{i=1} u_i^B (R - R_e)^i \quad (10)$$

approximate both the adiabatic correction and homogeneous nonadiabatic mixing terms in the nuclear part of the diatomic Hamiltonian, while

$$q(R) = M_A^{-1} \sum_{i=0} q_i^A (R - R_e)^i + M_B^{-1} \sum_{i=0} q_i^B (R - R_e)^i, \quad (11)$$

takes into account heterogeneous nonadiabatic mixing.

Results from a modified-Morse fit are displayed in Table 6. With 2184 transitions and eight adjustable parameters the standard deviation was 0.8858. The same weights assigned to the transitions for the Dunham fit, discussed above, were also used in the modified-Morse fit yielding residuals that were essentially identical to those of the Dunham fit (Tables 1–3). A few minor changes made to the data set of this fit are worth noting. Millimeter-wave data for $v > 34$, the last seven entries in Table 3, were excluded since the residuals of these transitions from trial fits were consistently 8–25 times greater than their estimated weights (eq. [4]). Furthermore, because pure rotational transitions do not convey any direct information about the spacing of vibrational levels, that is critical toward

TABLE 5
MASS-DEPENDENT DUNHAM CONSTANTS^a

	²⁸ SiO	²⁹ SiO	³⁰ SiO
This work			
Y_{10}	1241.543934(55)	1233.729913(54)	1226.408414(54)
Y_{20}	-5.9744973(194)	-5.8995295(192)	-5.8297164(190)
$10^3 Y_{30}$	6.10438(247)	5.98984(242)	5.88384(238)
$10^5 Y_{40}$	-1.1586(100)	-1.12974(975)	-1.10316(952)
Y_{01}	0.7267522517(380)	0.7176329819(376)	0.7091407525(371)
$10^3 Y_{11}$	-5.03808526(941)	-4.94355670(924)	-4.85606621(907)
$10^6 Y_{21}$	2.51440(187)	2.45169(182)	2.39401(178)
$10^8 Y_{31}$	-1.8871(115)	-1.8284(111)	-1.7748(108)
$10^{10} Y_{41}$	-1.9095(201)	-1.8385(193)	-1.7740(187)
$10^7 Y_{02}$	-9.96081707	-9.71240923	-9.48390249
$10^{10} Y_{12}$	-4.13182855	-4.00343059	-3.88604152
$10^{11} Y_{22}$	-1.85735842	-1.78831381	-1.72557520
$10^{13} Y_{32}$	-2.54333503	-2.43337806	-2.33407483
$10^{14} Y_{03}$	3.57661163	3.44365629	3.32284404
$10^{15} Y_{13}$	-7.93577518	-7.59268480	-7.28283647
$10^{16} Y_{23}$	-1.23349256	-1.17273680	-1.11820329
$10^{18} Y_{33}$	-1.38793433	-1.31126641	-1.24287135
$10^{18} Y_{04}$	-1.04752522	-0.99592929	-0.94961752
$10^{20} Y_{14}$	-3.17887927	-3.00328158	-2.84663178
$10^{22} Y_{24}$	-7.97091177	-7.48321156	-7.05079830
$10^{24} Y_{05}$	-2.25836160	-2.12018376	-1.99767011
$10^{25} Y_{15}$	-1.39217508	-1.29876890	-1.21645815
$10^{27} Y_{25}$	-3.38996222	-3.14261287	-2.92597900
$10^{30} Y_{06}$	-8.90143877	-8.25194330	-7.68310125
$10^{31} Y_{16}$	-6.93051289	-6.38438992	-5.90901036
$10^{35} Y_{07}$	-3.34583732	-3.06278739	-2.81791070
$10^{36} Y_{17}$	-2.95232723	-2.68555793	-2.45617850
$10^{40} Y_{08}$	-1.41202050	-1.27634780	-1.16040466
$10^{46} Y_{09}$	-5.94970017	-5.31054532	-4.77100203
Glenar et al. (1985)			
Y_{10}	1241.54252(27)	1233.72857(27)	1226.40712(27)
Y_{20}	-5.97401(11)	-5.89905(11)	-5.82924(11)
$10^3 Y_{30}$	6.024(17)	5.911(17)	5.807(17)
$10^5 Y_{40}$	-0.775(88)	-0.755(85)	-0.737(83)
Y_{01}	0.72675182(6)	0.71763263(6)	0.70914045(6)
$10^3 Y_{11}$	-5.03778(6)	-4.94326(6)	-4.85578(5)
$10^6 Y_{21}$	2.365(13)	2.306(12)	2.251(12)
$10^7 Y_{02}$	-9.893(6)	-9.646(6)	-9.419(6)
$10^{10} Y_{12}$	3.4(4)	3.3(3)	3.2(3)
$10^{12} Y_{03}$	1.0	1.0	1.0

^a In units of cm⁻¹.

[11]), failed to further improve the quality of the modified-Morse fit. The Coriolis term in the rotational Hamiltonian, $-B(R)(J_+L_- + J_-L_+)$, where $B(R) = \hbar^2/2\mu R^2$, can only couple rotational levels of ${}^1\Sigma$ to those of ${}^1\Pi$ states. In our model this type of interaction is taken into account by the $q(R)$ function. In most circumstances, the power series expansion form for $q(R)$ is adequate; that is, when the condition of large ${}^1\Sigma-{}^1\Pi$ energy separation is well satisfied. In the case of SiO the first excited $A^1\Pi$ state lies 42800 cm⁻¹ above the ground state (Huber & Herzberg 1979). Term energies for $v \leq 13$ rotational levels are less than 20000 cm⁻¹. The fact that levels for $v \leq 13$ were not sensitive to $q(R)$ is not surprising. However, the $v = 40$, $J = 8$ level, for instance, lies at 40900 cm⁻¹, which is considerably closer to the manifold of $A^1\Pi$ rotational levels. An indication of a strong Coriolis interaction between rovibrational levels of $X^1\Sigma^+$ with those of $A^1\Pi$ is a long and slowly converging $q(R)$ expansion. Because the trial fits failed to determine even the parameters for the lowest terms in the $q(R)$ expansion, aside from q_0 which is discussed above, tends to rule out any significant $X^1\Sigma^+-A^1\Pi$ interaction.

The rotational magnetic moments g_J determined by Davis & Muenster (1974) for the first three vibrational levels of ²⁸Si¹⁶O in the $X^1\Sigma$ state provide a consistency check of our analysis. The rotational moment consists of an angular momentum contribution due to nuclear charges, g_J^N , independent of internuclear separation, and the electronic contribution,

$$g_J^e = -\mu_N B_e \sum_n \frac{|\langle n^1\Pi | L_+ | {}^1\Sigma \rangle|^2}{E(n^1\Pi) - E({}^1\Sigma)}. \quad (12)$$

The vibrational dependence of g_J can be examined by expanding the radial dependence of the rotational moment in a power series about the equilibrium internuclear separation R_e ,

TABLE 6
DERIVED PARAMETER VALUES FOR THE
MODIFIED-MORSE POTENTIAL^a

D_e (cm ⁻¹)	66620.0
R_e (Å)	1.997371600(360)
β_0	5.6424370514(545)
β_1	4.781647998(354)
β_2	7.0745599(485)
β_3	12.432657(187)
β_4	20.48944(788)
β_5	36.4352(415)
β_6	0.0
β_7	566.118(208)
$M_{\text{Si}}(28)$ (u)	27.9769271
$M_{\text{Si}}(29)$ (u)	28.9764949
$M_{\text{Si}}(30)$ (u)	29.9737707
$M_{\text{O}}(16)$ (u)	15.99491463

^a Uncertainties (numbers in parentheses) are quoted to 1σ . Standard deviation of the fit was 0.8858 involving 2184 transitions. Range of integration, 1.0 Å $\leq R \leq 2.6$ Å; grid spacing, 0.0020 Å.

properly determining the values of β , the data set was supplemented with the five low-precision Bredohl et al. (1973) $\Delta G_{v+1/2}$ separations for $23 \leq v \leq 27$ (see Barrow & Stone (1975) for correct assignments) as shown in Table 7. The dissociation energy D_e was held fixed to the mass spectrometry value quoted in Huber & Herzberg (1979) while isotopic masses of silicon and oxygen were obtained from Mills et al. (1989). The u_i^{Si} and q_i^{Si} parameters for $i > 0$ (eqs. [10] and [11]) were not determined. Because of high correlation between q_0^{Si} and R_e , varying q_0^{Si} or fixing it to zero had no effect on the quality of the fit; we decided instead to fix q_0^{Si} to zero with the effects of this term being absorbed completely by the adjustable internuclear separation parameter R_e .

Attempts of adding correction terms to the rotational part of the Hamiltonian, the $q(R)$ function for the silicon center (eq.

TABLE 7
BREDOHL ET AL. (1973) VIBRATIONAL DATA

v	$\Delta G_{v+1/2}$ (cm $^{-1}$)	Barrow & Stone (1975)	Observed-Calculated		
			Dunham ^a	Modified-Morse Potential ^b	Weight (cm $^{-1}$)
23	964.69	0.07	0.01	0.02	0.05
24	953.55	0.06	0.01	0.01	0.05
25	942.28	-0.11	-0.16	-0.15	0.20
26	931.37	0.05	0.01	0.02	0.05
27	920.22	-0.08	-0.09	-0.08	0.10

^a Predicted using Dunham U constants in Table 4.

^b Least-squares residuals.

$$g_J^e(R) = g_J^e(R_e) + \left(\frac{dg_J^e}{dR} \right)_{R=R_e} (R - R_e) + \frac{1}{2} \left(\frac{d^2 g_J^e}{dR^2} \right)_{R=R_e} (R - R_e)^2 + \dots \quad (13)$$

With the modified-Morse vibrational wavefunctions a fit of the Davis & Muenter g_J values to the expectation values of equation (13) gave

$$g_J(R_e) = -0.153150(8), \\ \left(\frac{dg_J^e}{dR} \right)_{R=R_e} = -0.1126(6) \text{ \AA}^{-1}.$$

By expressing $g_J(R)$ relative to the nuclear centers (Watson 1973),

$$g_J(R) = [(\tilde{g}_0^{\text{Si}} + \tilde{g}_1^{\text{Si}}(R - R_e)]M_{\text{Si}}^{-1} + [\tilde{g}_0^{\text{O}} + \tilde{g}_1^{\text{O}}(R - R_e)]M_{\text{O}}^{-1}, \quad (14)$$

yields $\tilde{g}_0^{\text{Si}} = -1.01266(8)$, $\tilde{g}_1^{\text{Si}} = -0.712(6) \text{ \AA}^{-1}$, $\tilde{g}_0^{\text{O}} = -1.87067(8)$, and $\tilde{g}_1^{\text{O}} = -1.394(6) \text{ \AA}^{-1}$, using the dipole moment function discussed in the next section. In accordance with equation (11),

$$q_i^{\text{Si(O)}} \simeq \frac{m_e}{m_p} \tilde{g}_i^{\text{Si(O)}}. \quad (15)$$

Thus,

$$q_0^{\text{Si}} \simeq -5.5151(4) \times 10^{-4}, \\ q_1^{\text{Si}} \simeq -3.88(3) \times 10^{-4} \text{ \AA}^{-1}, \\ q_0^{\text{O}} \simeq -1.01880(4) \times 10^{-3}, \\ q_1^{\text{O}} \simeq -7.59(4) \times 10^{-4} \text{ \AA}^{-1}.$$

For comparison, the parameters for isovalent CO (Coxon & Hajigeorgiou 1992) are $q_2^{\text{C}} = -2.64 \times 10^{-3} \text{ \AA}^{-2}$, and $q_1^{\text{O}} = -3.36 \times 10^{-3} \text{ \AA}^{-1}$.

Analysis of the low- v rotational moments indicates modest J -dependent Born-Oppenheimer breakdown on the silicon center, in discord with the modified-Morse fit. The key to reconciling these seemingly opposite conclusions is to realize that without informative isotope data, the nonadiabatic corrections are inseparable from the Born-Oppenheimer portion of the internuclear potential. The vast portion of the data set used in this work consists predominantly of ^{28}SiO lines (80%). Moreover, only the $v = 0$, $J = 0 \rightarrow 1$ microwave transitions have been measured for the minor isotopomers to an accuracy of 90 kHz, just short of the accuracy of 30 kHz needed in unveiling the $q(R)$ contribution to the isotope shift. On the other hand, the minor isotopomer IR line positions with uncertainties of 24–30 MHz are far too coarse to reveal the subtle 0.03–10 MHz isotope shifts induced by $q(R)$. As a result, the modified-Morse potential determined by the fit is essentially an effective ^{28}SiO internuclear potential. For the purpose of predicting transitions in pure rotation and IR spectra from astronomical sources, this does not pose a serious limitation since the prominent spectral features will always involve the predominantly abundant ^{28}SiO isotopomer.

To clarify a point made earlier, concerning the proximity of the $A^1\Pi$ state to the rotational levels in the high vibrational states, the lack of isotope information makes it virtually impossible to assess the extent of J -dependent breakdown in these levels. Because $X^1\Sigma^+$ and $A^1\Pi$ (along with a host of other electronic states) dissociate to the same limit, $\text{Si}({}^3P) + \text{O}({}^3P)$, it stands to reason that a dramatic enhancement of J -dependent breakdown should occur as their potential curves begin to merge around $R = 3 \text{ \AA}$. The abrupt change in the modified-Morse potential, signified by the anomalous values for β_6 and β_7 that lead to a premature flattening of the outer wall of the potential for $R > 2.2 \text{ \AA}$, may in fact be an indication of mutual repulsion of the $X^1\Sigma^+ - A^1\Pi$ levels. A follow-up to the Mol-laaghbab et al. millimeter-wave study involving isotope enriched ^{29}Si , ^{30}Si , and perhaps ^{18}O silicon monoxide is therefore needed in quantifying the J -dependent $A^1\Pi$ mixing in the higher-lying rovibrational levels of $X^1\Sigma^+$.

One other important effect that we have not yet fully discussed is homogeneous nonadiabatic Born-Oppenheimer breakdown (eq. [10]) which in this case treats the cumulative

interactions of distant ${}^1\Sigma^+$ states. According to Langhoff & Arnold (1979), their SCF + CI calculation indicates that the dominant configuration for $X{}^1\Sigma^+$ for R close to R_e is $5\sigma^26\sigma^27\sigma^22\pi^4$ while the single promotion, $2\pi \rightarrow 3\pi$, and a number of lesser double promotions influence the configurational ordering of orbitals as the asymptotic limit toward dissociation is approached. (Note that 2π and 3π are essentially oxygen- and silicon-centered $2p$ and $3p$ orbitals, respectively.) Another SCF-CI study by Robbe et al. (1979) focused more attention on the excited $E{}^1\Sigma^+$ state. According to these authors the E state cannot be represented by a single configuration, but by a mixture of three configurations, two of which are $5\sigma^26\sigma^27\sigma^22\pi^4$ and $5\sigma^26\sigma^27\sigma^22\pi^33\pi$. Furthermore, both of these studies support the notion that $E{}^1\Sigma^+$ dissociates to $\text{Si}({}^3P) + \text{O}({}^3P)$. In view of these results, enhancement of homogeneous breakdown in the high-lying rovibrational levels of $X{}^1\Sigma^+$ by $E{}^1\Sigma^+$ is a very likely possibility.

The present minor isotopomer IR data is adequate in ruling out a significant homogeneous nonadiabatic interaction occurring in the vibrational levels up to $v = 6$. To assess the extent of this interaction in the higher levels, IR spectra for a number of isotopomers in the region above $v = 13$ is preferred since rovibrational transitions, unlike pure rotational transitions, would give direct information about the contribution of this interaction to the vibrational isotope shifts. However, spectra from sunspots offer very little hope here; first overtone hot bands are much too weak to detect beyond $v = 13$. A remote possibility may lie in detecting higher overtone hot bands in the spectra of sunspots or in the cooler photospheres of late-type stars. A more likely laboratory source for generating such spectra may be the microwave discharge.

Further studies are needed to characterize better the internuclear potential out to larger internuclear separations to clarify questions raised in this investigation regarding the interaction of $X{}^1\Sigma^+$ with neighboring excited electronic states. Results from these studies would have important implications in devising an intramolecular energy transfer model for SiO which may be instrumental in settling the controversy surrounding the underlying mechanism responsible for stellar and interstellar masers.

3.3. RKR and Dunham Potentials

Rovibrational intensities of SiO are of considerable importance to astrophysicists in connection with detection and simulation of microwave and IR emission spectra in stellar and interstellar media. Ab initio calculations by Langhoff & Arnold (1979) and numerous subsequent studies (Langhoff & Bauschlicher [1993] and references therein) have yielded dipole moment functions $M(R)$ for internuclear separations extending out to 5 Å. Tipping & Chackerian (1981) developed an empirical formula for $M(R)$ in the form of a Padé approximant which was based largely on the highly accurate Raymonda et al. (1970) experimental dipole moments for the four lowest vibrational levels. An accurate electric-dipole moment function is essential to computing Einstein A -coefficients,

$$A = \frac{64\pi^4}{3h} v^3 \frac{|\Delta(J(J+1)|}{2J'+1} |\langle v, J | M(R) | v', J' \rangle|^2. \quad (16)$$

TABLE 8
DUNHAM POTENTIAL PARAMETERS

	Dunham U Constants	Modified-Morse Potential
a_0 (cm $^{-1}$)	530246.4965(543)	530246.83187(676)
a_1	-2.97380199(369)	-2.9737747785(162)
a_2	5.5738281(327)	5.5737826225(640)
a_3	-8.284755(308)	-8.28744383(213)
a_4	10.54009(295)	10.5652177(156)
a_5	-11.8361(210)	-11.9359857(571)
a_6	11.468(134)	11.737323(736)
a_7	-5.818(831)	-6.90675(404)
R_e (Å)	1.509737502(395)	1.5097371600(360)

However, recent observations of α Tau have raised concerns about the accuracy of computed Einstein A -coefficients reported so far (Langhoff & Bauschlicher 1993).

Previous methods for computing Einstein A -coefficients relied heavily upon first-order RKR analysis, analytical perturbation techniques, or even a combination of both in evaluating $\langle v, J | M(R) | v', J' \rangle$. RKR methods utilize molecular constants rather than actual data in generating inner and outer turning points of the internuclear potential. The radial Schrödinger equation is then solved numerically using the discrete set of RKR turning points to obtain radial wave functions that are in turn employed in the numerical evaluation of the dipole moment integrals.

Analytical methods are based on perturbation theory and rely on the properties of the Dunham potential to generate radial moments directly without having to solve the Schrödinger equation.⁴ The best example of this type of technique is the one outlined by Tipping (1973) where he was able to derive a general recursion relation for generating radial moments starting from the hypervirial theorem. Although analytical techniques are considered to be highly accurate and reliable, numerical techniques tend to be more efficient and practical, and in many cases rival analytical methods in terms of accuracy. For those who find these analytical methods appealing, we list in Table 8 two sets of Dunham potential constants, the first set which was derived from the Dunham U_{i0} 's and U_{i1} 's, and the second set which was obtained by expanding the modified-Morse function in a power series about B_e .

With the molecular constants listed in Table 4, we generated first-order RKR inner and outer turning points for the $J = 0$ vibrational levels up to $v = 40$ and plotted them along with the modified-Morse potential as shown in Figure 1; on this energy scale the agreement is excellent. A plot on a more sensitive scale, $[U^{RKR}(R) - U^{MMP}(R)]/U^{MMP}(R)$, as shown in Figure 2, indicates that the agreement is quite good over much of the range of internuclear separation where relative differences in the nearly flat region, $R > 1.3$ Å, amount to absolute energy differences of less than 1 cm $^{-1}$. The large discrepancies that occur at the inner points of the $v > 20$ levels do not necessarily reflect an inherent problem with the RKR method but are

⁴ As a requirement, the dipole moment function must be in a form of a power series expansion.

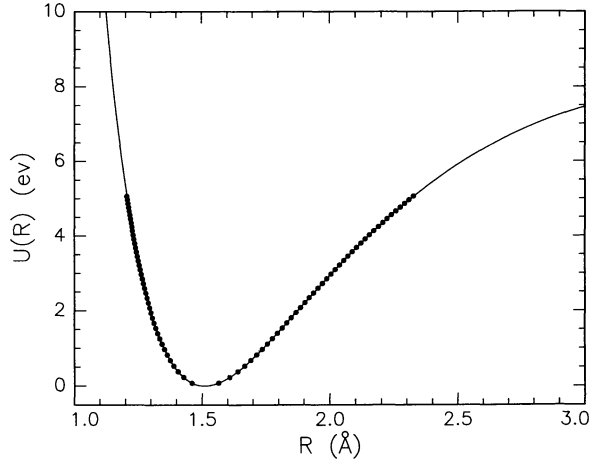


FIG. 1.—Comparison of the modified-Morse potential (solid curve) with the turning points from a RKR calculation (discrete points) for the first 40 $J = 0$ vibrational levels.

more likely due to an artifact of extrapolating vibrational energies outside the intended range where the vibrational constants are valid. The choice of using first-order RKR turning points over the modified-Morse function in obtaining vibrational wavefunctions leads only to slight inaccuracies in the Einstein A -coefficients.

To illustrate this, $\langle v|\xi|v'\rangle$ and $\langle v|\xi^2|v'\rangle$ moments in terms of the dimensionless Dunham coordinate, $\xi = (R - R_e)/R_e$, were calculated using both RKR and modified-Morse vibrational wave functions; the results in the form of relative differences are displayed in Figures 3 and 4. Using the modified-Morse vibrational wave functions a fit of the Raymonda et al. dipole moments to the expectation values of

$$M(\xi) = M(0) + \left(\frac{dM}{d\xi} \right)_{\xi=0} \xi \quad (17)$$

gave $M(0) = 3.0885(1)$ D and $dM/d\xi = 3.70(1)$ D. In the range $0 \leq v \leq 3$, where the linear approximation of the dipole

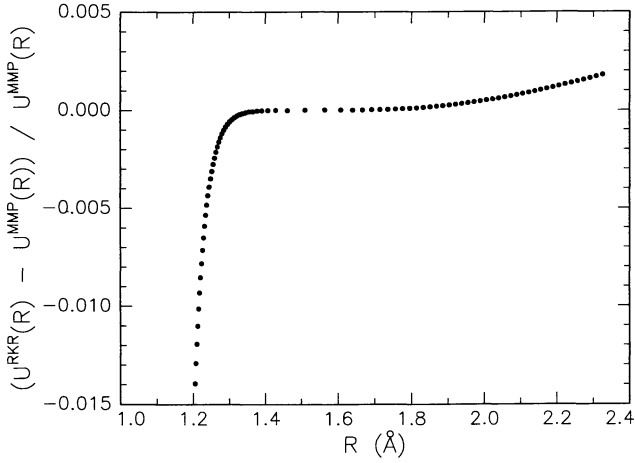


FIG. 2.—A plot of the RKR turning points relative to the values of the modified-Morse potential.

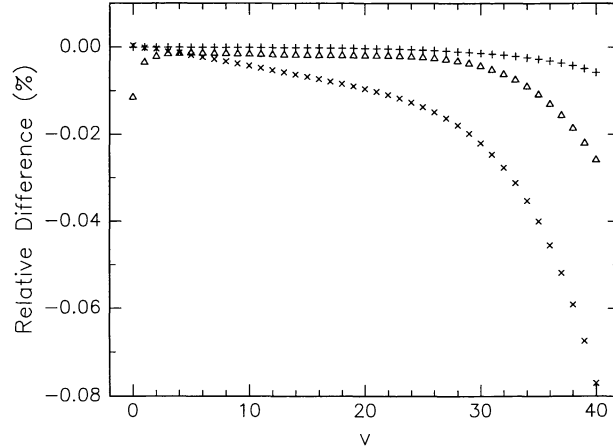


FIG. 3.—Relative differences between the RKR and modified-Morse $\langle v|\xi|v'\rangle$ moments for $\Delta v = v' - v = 0$ (open triangles), $\Delta v = 1$ (plus signs), and $\Delta v = 2$ (mult crosses).

moment function is valid, maximum errors in the Einstein A -coefficients are 0.02% for $\Delta v = 0, 1$, and 2. Lack of precise information about the sign and magnitude of successive higher order derivatives of $M(R)$ precludes the possibility of reliably estimating the errors for higher vibrational levels. However, if the trends in the relative differences for the first and second moments are any indication, then the relative errors in the Einstein A -coefficients are expected to remain less than 1% for higher v , at least as far as using RKR versus modified-Morse radial wave functions are concerned.

4. CONCLUSION

Astronomical sources such as “cool” stellar atmospheres, circumstellar shells or even sunspots are attractive as alternate sources for recording high-resolution IR spectra of high-temperature molecules. The favorable conditions that exist in these sources for forming high-temperature molecules are not particularly easy, and in many instances impossible, to dupli-

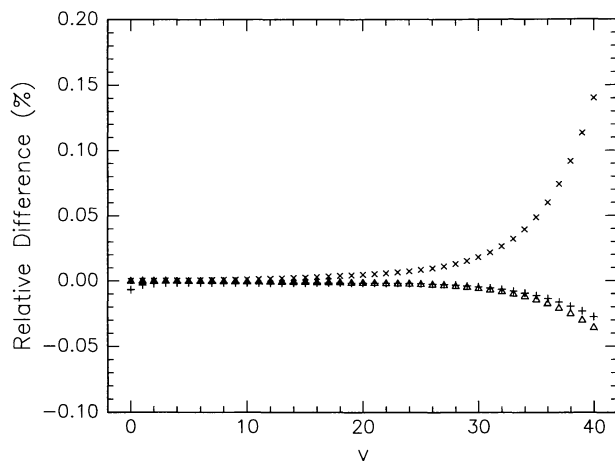


FIG. 4.—Relative differences between the RKR and modified-Morse $\langle v|\xi^2|v'\rangle$ moments for $\Delta v = v' - v = 0$ (open triangles), $\Delta v = 1$ (plus signs) and $\Delta v = 2$ (mult crosses).

cate in the laboratory. The FTS IR sunspot spectrum of SiO reported here is a case in point. Over 1700 measured lines were collected from our sunspot spectra, which even surpasses the collection of almost 1000 IR lines measured by Glenar et al. (1985) from a FT sunspot spectrum as well. The comprehensive data set assembled from this spectrum consisted of lines from the vibrationally consecutive (1, 0) to (13, 12) bands for ^{28}SiO and (1, 0) to (6, 5) bands for ^{29}SiO and ^{30}SiO involving rotational levels as high as $J = 141$. Nevertheless, the much lower temperature laboratory spectrum that we recorded still served the two useful purposes of filling in *R*-branch lines masked in the sunspot spectrum by the absorption of Earth's atmosphere and providing a straightforward way of calibrating the sunspot lines to rest frequencies. It is worth emphasizing that neither resolution nor accuracy had to be compromised in obtaining these spectra.

- Barrow, R. F., & Stone, T. J. 1975, *J. Phys. B*, 8, L13
 Beer, R., Lambert, D. L., & Sneden, C. 1974, *PASP*, 86, 806
 Bredohl, H., Cornet, R., Dubois, I., & Remy, F. 1973, *Canadian J. Phys.*, 51, 2332
 Campbell, J. M., Dulick, M., Klapstein, D., White, J. B., & Bernath, P. F. 1993, *J. Chem. Phys.*, 99, 8379
 Coxon, J. A., & Hajigeorgiou, P. G. 1991, *Canadian J. Phys.*, 69, 40
 Cudaback, D. D., Gaustad, J. E., & Knacke, R. F. 1971, *ApJ*, 166, L49
 Davis, R. E., & Muenter, J. S. 1974, *J. Chem. Phys.*, 61, 2940
 Dunham, J. L. 1932, *Phys. Rev.*, 41, 721
 Engels, D., & Heske, A. 1989, *A&AS*, 81, 323
 Gaur, V. P., Pande, N. C., & Tripathi, B. M. 1972, *Bull. Astron. Inst. Czechoslovakiá* 24, 139
 ———. 1978, *Sol. Phys.*, 56, 67
 Geballe, T. R., Lacy, J. H., & Beck, S. C. 1979, *ApJ*, 230, L47
 Geballe, T. R., & Townes, C. H. 1974, *ApJ*, 191, L37
 Glenar, D. A., Deming, D., Jennings, D. E., Kostiuk, T., & Mumma, M. J. 1983, *ApJ*, 269, 309
 Glenar, D. A., Hill, A. R., Jennings, D. E., & Brault, J. W. 1985, *J. Mol. Spectrosc.*, 111, 403
 Hinkle, K. H., Barnes, T. G., Lambert, D. L., & Beer, R. 1976, *ApJ*, 210, L141
 Huber, K. P., & Herzberg, G. 1979, *Constants of Diatomic Molecules* (New York: Van Nostrand-Reinhold)
 Kwan, J., & Scoville, N. 1974, *ApJ*, 194, L47
 Langhoff, S. R., & Arnold, J. O. 1979, *J. Chem. Phys.*, 70, 852
 Langhoff, S. R., & Bauschlicher Jr., C. W. 1993, *Chem. Phys. Lett.*, 211, 305

Molecular constants for the $X^1\Sigma$ state in the form of mass-reduced Dunham *U* constants were derived from the analysis that incorporated pure rotational data from several sources. This set of constants, the most accurate to date, should be instrumental in assignment or simulation of astronomical microwave, millimeter-wave, and IR spectra. Also derived from the analysis was an intermolecular potential in the form of a modified-Morse function.

This work was supported by the Natural Sciences and Engineering Research Council of Canada (NSERC). Acknowledgment is made to the Petroleum Research Fund, administered by the American Chemical Society, for partial support of this work. We also wish to thank the NASA Laboratory Astrophysics Program for additional support. We thank R. Mollaaghbabá for sending us the SiO millimeter wave line list.

REFERENCES

- Lovas, F. J., Maki, A. G., & Olson, W. B. 1981, *J. Mol. Spectrosc.*, 87, 449
 Manson, E. L., Clark, W. W., De Lucia, F. C., & Gordy, W. 1977, *Phys. Rev. A*, 15, 223
 Mills, I., Cvitaš, T., Homann, K., Kallay, N., & Kuchitsu, K. 1988, *Quantities, Units, and Symbols in Physical Chemistry* (Oxford: Blackwell)
 Mollaaghbabá, R., Gottlieb, C. A., Vrtilek, J. M., & Thaddeus, P. 1991, *ApJ*, 368, L19
 Ogilvie, J. 1983, *Comput. Phys. Commun.*, 30, 101
 Raymonda, J. W., Muenter, J. S., & Klemperer, W. A. 1970, *J. Chem. Phys.*, 52, 3458
 Rinsland, C. R., & Wing, R. F. 1982, *ApJ*, 263, 201
 Robbe, J. M., Schamps, J., Lefebvre-Brion, H., & Raseev, G. 1979, *J. Mol. Spectrosc.*, 74, 375
 Ross, A. H. M., Eng, R. S., & Kildal, H. 1974, *Opt. Commun.*, 12, 433
 Snyder, L. E., & Buhl, D. 1974, *ApJ*, 189, L31
 Tipping, R. H. 1973, *J. Chem. Phys.*, 59, 6433
 Tipping, R. H., & Chackerian Jr., C. 1981, *J. Mol. Spectrosc.*, 88, 352
 Töring, T. 1968, *Z. Nat.*, 23A, 777
 Tyuterev, V. G., & Velichko, T. J. 1984, *Chem. Phys. Lett.*, 104, 596
 Wallace, L., Livingston, W., & Bernath, P. 1994, *National Solar Obs. Tech. Rep.*, No. 1994-01,
 Watson, J. K. G. 1973, *J. Mol. Spectrosc.*, 45, 99
 ———. 1980, *J. Mol. Spectrosc.*, 80, 411
 Wilson, R. W., Penzias, A. A., Jefferts, K. B., & Kutner, M., & Thaddeus, P. 1971, *ApJ*, 167, L97
 Wollman, E. R., Geballe, T. R., Greenberg, L. T., Holtz, J. Z., & Rank, D. M. 1973, *ApJ*, 184, L85